Numerical Study of Shock-Wave Boundary Layer Interaction on a Compression Ramp Gap

A Thesis Presented for the

Master of Science

Degree

The University of Tennessee, Knoxville

Andrew Brandon Bell

May 2018

I would like to dedicate this work to my family and friends for their endless love and support.

Acknowledgments

I would like to thank Dr. Trevor Moeller, my professor and advisor, for introducing me to UTSI, taking me into his research group, and providing the topic of this research. I would also like to thank Dr. Greg Power and Dr. Steve Brooks for guidance and taking their time be on my committee. Many thanks are due to Adam Croft who beared the brunt of my trivial CFD and software operation questions. I have to thank my mother, Nancy Bell; Ronnie Bounds; and my grandmother, Barbara Bell for encouraging and supporting from a young age an interest in science, engineering, and aerospace while pushing me to work hard and perservere. Finally, I would like to thank my wife, Mallory, for being my companion through everything and always supporting me.

Abstract

The effect of a gap between a flat plate and a compression ramp on the shock wave/boundary layer interaction (SWBLI) at the ramp corner is investigated numerically. The behavior of supersonic flow over compression ramps where SWBLI occurs has been a topic of study, numerically and experimentally, for many years. There have been studies on how the interaction occurs and how to mitigate its effects. This investigation will focus on the effect of placing a gap in front of the ramp.

Using ANSYS Fluent and a Spalart-Allmaras turbulence model, two 3D models experience Mach 3 flows at a ramp angle of 24° with and without a gap. Steady state simulations highlight the characteristic features of SWBLIs on compression ramps (separation point, reattachment point, and recirculation region) and how these features are altered by the presence of the gap. Span-wise averaging is performed to represent pressure, temperature, and skin friction surface data, and these data are used to analyze the effect of the gap. The hypothesis is that the addition of the gap will lower the negative effect of the SWBLI on the surface. Additional test cases are created to observe the effect of angle of attack change, boundary layer height change, and Mach number change on the gap.

With the addition of the gap, the SWLBI recirculation region is found to move from the corner into the gap and the shock impinges directly from the corner of the ramp. This changes the location of pressure and temperature loading on the surfaces. The average temperature is lower with the addition of the gap, but the amount of pressure loading across the surfaces stays within 1%. The pattern of skin surface friction on the ramp, however, changes dramatically when the gap is added. The skin friction coefficeint value decreases by 100% at top of the ramp when the gap is added. The present research introduces and

investigates a scarcely covered technique to help mitigate or control the effects of SWBLI on a compression ramp and addresses possible work to follow-up this study.

Table of Contents

List of Tables

List of Figures

Nomenclature

α	Angle of Attack
δ_0	Boundary Layer Height
$\dot{m}$	Mass Flow Rate
γ	Specific Heat Ratio
ρ	Density
A	Area
C_f	Coefficient of Friction
M_∞	Freestream Mach Number
P	Static Pressure
P_0	Total Pressure
P_w	Wall Pressure
Re_δ	Reynolds Number
T	Static Temperature
T_0	Total Temperature
U_∞	Freestream Velocity

Chapter 1

Introduction

As humans use technological advancements and feats of engineering prowess to force man-made vehicles faster and faster in the atmosphere, there exists an ongoing struggle to understand the physics of what happens to metal and composite objects at these high speeds. The study of supersonic speed is not recent; it began even before the first manned flight [14]. However, the physical phenomena that occur during high Mach flight are still the subject of rigorous investigation.

The cost associated with a supersonic or hypersonic vehicle design process is prohibitive for running a large number of real-time flight tests. Even ground testing in wind-tunnels can require a large amount of resources. This is where computational fluid dynamics (CFD) provides a much-needed benefit to the field. Though not as accurate as true flight test, CFD has provided an incredible wealth of knowledge into the behavior of flow in supersonic flight, specifically turbulence and shockwaves. The advances in computational simulation power and wind-tunnel test diagnostics over the last few decades have created breakthroughs in these fields and allow for broader study of physical trends and more in-depth examinations into specific behaviors of fluid flow in the supersonic and hypersonic regimes [8] [9] [26] [33].

One of the reoccurring phenomena worth evaluating is shock-wave boundary layer interaction (SWBLI). As the name suggests, this interaction is the result of an incoming boundary layer entering into a shock-wave. This interaction can occur in a number of ways on different geometric configurations; but the overall trends are similar, and the effect on the object where the SWBLI is created must be understood. There are negative effects

associated with SWBLI, such as large-scale unsteadiness [11], increased local skin friction [21], and increased temperature and pressure [19]. Many methods have been created to mitigate the interaction's influence, such as mass injection [35] [36], distributed suction [20], local suction [24], and vortex generation [13] [25]. One method, examined here, is the introduction of a gap on a compression ramp in supersonic flow.

1.1 Motivation

The primary goal of the current work is to understand the effect of adding a small gap at the corner of a compression ramp that experiences supersonic fluid flow. Existing literature and preliminary investigations have shown that the SWBLI induced recirculation region at the foot of compression ramp without a gap disappears from the corner when a gap is added. [22] The recirculation region instead forms inside the gap between flat plate and ramp. The work of Gieseking et al. [19] serves as the groundwork for building the geometry and simulations created here and is used as a point of comparison for the results of those simulations. The design process, implementation, and testing of the gap are documented thoroughly. To understand the effectiveness of the gap addition the cases with and without the gap are compared under the same conditions. The following objectives are set herein:

1.1.1 Objective 1.

Using CFD, duplicate the results of Gieseking et al. [19] to validate domain setup and computational methods. The model indicated will be recreated to ensure correct geometry setup, meshing techniques, boundary conditions, initial conditions, turbulence model choice, and simulation methodology. Data provided in [19] will be compared to the results of original simulations to validate setup.

1.1.2 Objective 2.

Add a gap at the foot of the compression ramp used in Objective 1 and compare the results of flow past the compression ramp with and without the gap. To do this, the domain

used in Objective 1 will be edited to include a region beneath the flat plate and ramp. This will constitute the "No Gap" case. Then this new geometry will be edited to add the gap between the flat plate and ramp. This will be the "Gap" case. These two cases will be compared to examine the effect of the gap on SWBLI. Three variables will be studied in this comparison: pressure, temperature, and skin friction coefficient.

1.1.3 Objective 3.

Examine the effect of the gap when the boundary layer height, angle of attack, and Mach number are changed. Another set of new domains will be created with a leading edge tip. A series of tests will be applied to see how the gap affects change under different flow conditions. The flow direction will be changed to give an angle of attack (α) of 2.5° and 5° to the models. The boundary layer will be grown only from the leading edge. Also, the Mach number will be increased from Mach 3 to Mach 5. Again, the effects of the gap will be shown, and the Gap case and No Gap case will be compared during each test.

This thesis is as follows. Chapter 2 contains a literature review. Chapter 3 describes the process of duplicating the results of the Gieseking et al. [19] and shows the results of that work and the mimicked case. A description of what information will be carried on from duplicating the work is given. Chapter 4 introduces the full domain and compares the results of simulations with and without a gap in the corner of a compression ramp. Chapter 5 documents how the gap effects react to boundary layer height change, Mach number change, and increases in angle of attack. Finally, Chapter 6 provides conclusions and ideas for future work in this research area.

Chapter 2

Literature Review

As mentioned in Chapter 1, the study of SWBLI has been extensive in the last 50 years both experimentally and computationally. An overview of what SWBLI is and some of the history of SWBLI research is presented, specifically, research in SWBLI at compression ramp corners. A critical journal article presented by Gieseking et al. [19] will be presented. That study is the building block for this research, and their motivations, process, and results will be discussed, along with its connection to the research reported herein.

2.1 Background

SWBLI is a phenomenon found in the boundary layer, a region where viscosity is an essential part of the flow characteristics. When a viscous fluid passes over a surface there is a decrease in velocity from the freestream velocity to zero velocity at the wall. Concurrently, the Mach number of the flow also decreases to zero. [11] SWBLI occurs when an incoming boundary layer on a surface in a transonic, supersonic, or hypersonic flow comes into contact with the shockwave produced by another impinging shock, ramp, control surface, fin or any other protrusion on the surface in a flow field [7]. When flow crosses a shockwave, the Mach number and velocity sharply decreases, while temperature, density and pressure dramatically increase. Depending on conditions like shock angle and incoming Mach number, SWBLI will almost always result in a separated flow region. The separation is most commonly determined to be a result of an adverse pressure gradient being forced upon the boundary layer by the

flow behind the shockwave. There is a natural unsteadiness to this phenomenon and repeated oscillations in pressure and thermal loading on a surface can be damaging. [7][11]

SWBLI are prevalent in some capacity on every flow in the transonic, supersonic, and hypersonic regimes. Applications that can be affected by SWBLI include turbomachinery; supersonic engine inlets, such as scramjet and ramjet engines [30]; missiles; re-entry vehicles [11]; and external aerodynamic surfaces and control surfaces on high-speed vehicles. [7] The characterization of SWBLI and the understanding of its effects are a large part of high-speed flight vehicle design. SWBLI can affect material selection, thermal protection system design, geometry design, internal structure, and, ultimately, cost, time, and weight. [12]

2.2 Compression Ramps

The canonical geometries for SWBLI flows for experimental and computational study are the compression ramp, compression-expansion ramp, oblique incident/reflected shock, normal shock in a duct, blunt fin, and twin crossing shockwaves [7]. Figure 2.1 shows these examples. Each of these geometries or flow setups experience SWBLI, but the ways that the interactions occur are unique and are useful for study, each in their own right. In this research, only the compression ramp will be used.

In a supersonic flow, the compression ramp induces a shock which is a very strong adverse pressure gradient. The gradient then induces separation in the flow which propagates upstream. The growth of the separated section of flow causes a recirculation region in the corner. The location on the surface where separation occurs is called the separation point and the spot where the flow reconnects with the ramp is called the reattachment flow. These points are shown in Figure 2.2. This figure shows a SWBLI on a compression ramp and indicates where the separation is on the flat plate and the reattachment on the ramp. The strong shock that was initially impinged from the corner has now been spread out by the recirculation region. Compression waves first emanate from the flow at the separation point and coalesce into a separation shock-wave. Also, above the reattachment point a recompression shock is formed. These two shock-waves intersect and travel together farther into the flow. The size of the recirculation region and angle of the shockwave are determined

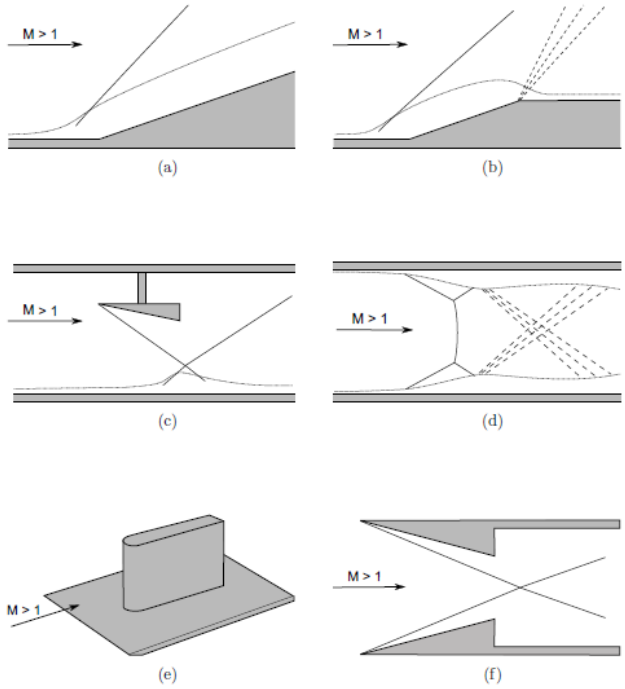

Figure 2.1: Canonical Geometries for SWBLI from [7] (a) Compression Ramp, (b) Compression-expansion Ramp, (c) Oblique Incident/Reflected Shock, (d) Normal Dhock in Duct, (e) Blunt Fin, and (f) Two Crossing Shock Waves.

by incoming boundary layer height, incoming Mach number, angle of the ramp, and Reynolds number. As boundary layer height increases, the recirculation region will, in turn, increase. Also as the ramp angle increases with constant Mach number, so will the recirculation region. However, with constant ramp angle and increasing Mach number, the recirculation region will shrink. [7]

2.3 Gieseking et al. Research

The research performed by Gieseking et al. [19] was crucial to the present work. Their simulation of a Mach 3, 24° compression ramp interaction served as the foundation for the research shown in the following chapters. Therefore, a brief description of what the study entails is necessary.

Gieseking et al created two large-eddy simulation/Reynolds-averaged Navier-Stokes (LES/RANS) [17] models and validated the results against previous experimental data.

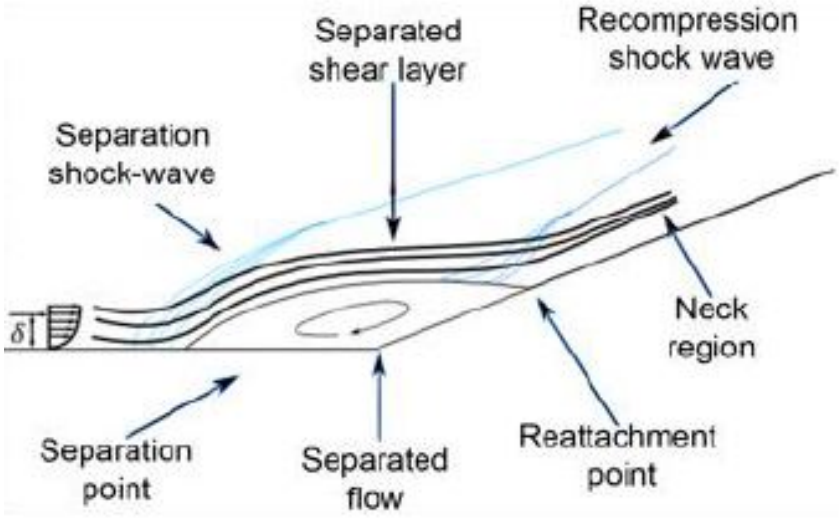

Figure 2.2: SWBLI Components on a Compression Ramp from [23].

LES/RANS models, also known as hybrid models, serve as a bridge between the computationally expensive but highly accurate LES turbulence method and the much less expensive, but less accurate, RANS method. Hybrid models use RANS in the boundary layer from the wall through the logarithmic section and switch to LES at the point where the boundary layer transitions to its wake like response. Figure 2.3 from [31] shows the different sections of a boundary layer. In boundary layer study, distance to the wall is measured with a non-dimensionalized value called y^+. This value is calculated by dividing the product of the friction velocity and the dimensionalized distance to the wall by the kinematic viscosity of the fluid. In the near wall region of $y^+ < 5$ the viscous sublayer existes and the velcoity profile is assumed to be laminar. Next, from $y^+ = 5$ to 30, a buffer region dominates. Here, both viscous and turbulent shear flows are found. Then, from around $y^+ = 30$ to 300, a log-law region persists where the flow becomes fully turbulent. At this point the boundary layer takes on a wake-like response as it approaches the velocity and turbulence of the freestream. [6]

The simulation created to test the models represented a compression ramp in a wind tunnel. There was a flat plate leading to a compression ramp of 24° and a large boundary layer of 0.025m existed on the flat plate. A recycling-rescaling method, originally introduced in Edwards et al. [15], was used to generate and maintain the incoming boundary layer on

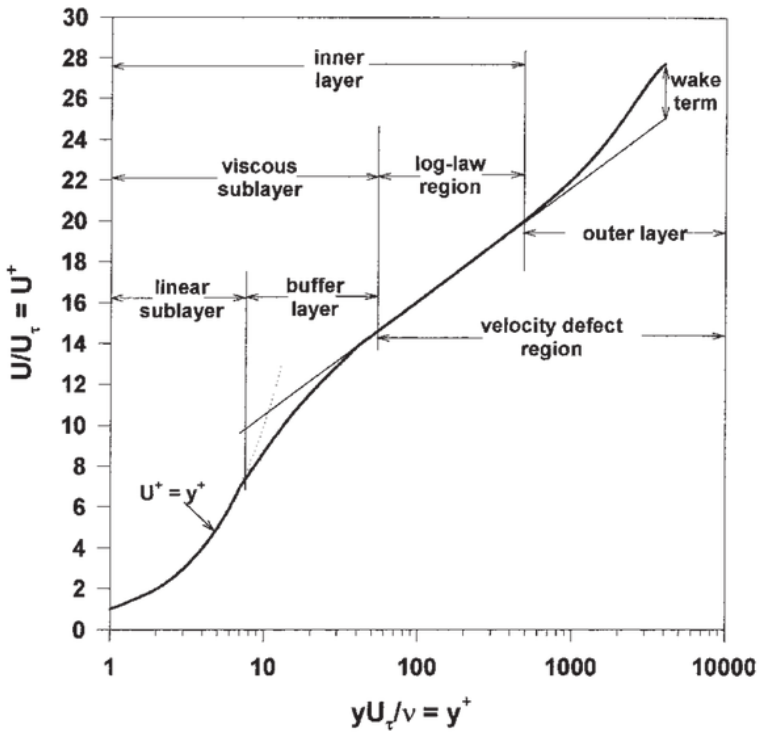

Figure 2.3: Sections of Boundary Layer [31].

the flat plate. In this method, a recycling plane is set up in the geometry and the during each time-step of the solution the instantaneous values of the flow are reproduced at the inlet. The results of the simulations were compared to another computation by Choi [10] and to experimental data collected by Settles et al. [32]. The study plotted velocity profiles through the interaction, surface pressure distributions, and surface skin friction distributions on the flat plate and ramp and compared the results of the simulations against the existing data points. In addition, an added image showed the flow field colored by temperature. This is shown in Figure 2.4. The area of high temperature in red and orange shows the SWBLI region.

The results of the study showed good agreement with the experimental data and the earlier simulation by Choi. The largest discrepancy came from an over-prediction of upstream influence in the recirculation, which allowed the recirculation region to grow by 15%, compared the experimental data. The research provided a foundation for the work shown in the following chapters. The geometry, boundary and flow conditions, initial mesh sizing, and boundary layer size were pulled from this research. The data for surface pressure distribution

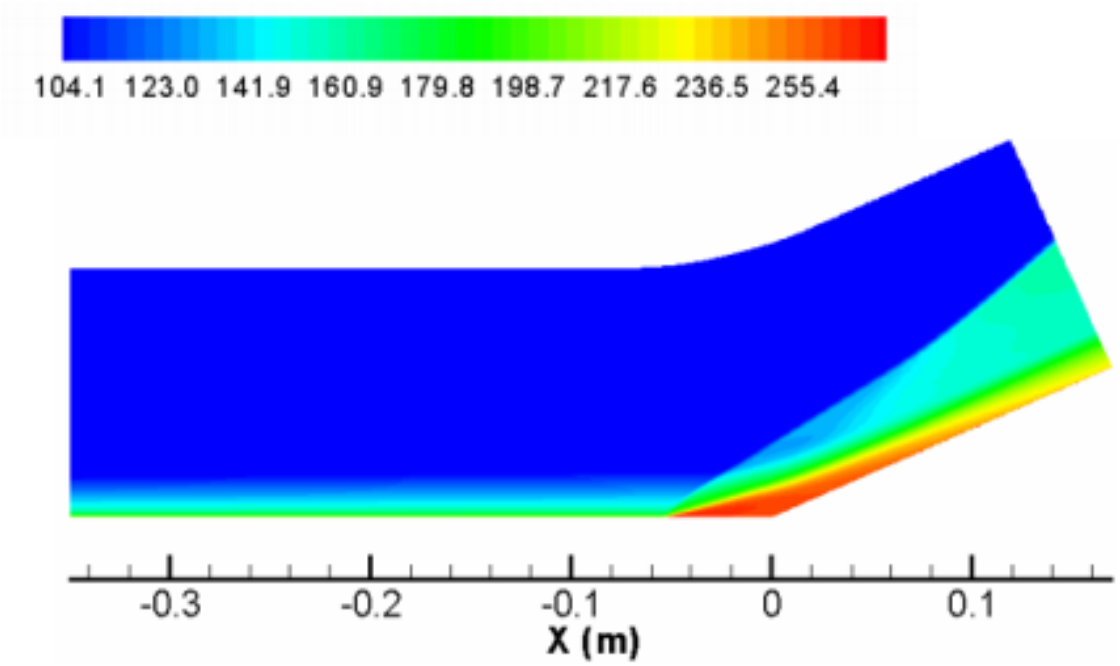

Figure 2.4: Temperature (K) Contours from [19].

and skin friction coefficient from Gieseking et al. [19], Settles et al. [32], and Choi [10] were pulled and used as a point of comparison for the work in Chapter 3.

2.4 Counter-rotating Vortex Research

A similar study to the work of Gieseking et al. in the previous section was performed by Edwards et al. [15]. Though, instead of Mach 3 flow, Mach 5 flow with a 28° ramp was used. The skin friction coefficient was, again, a point of study, but more time was spent investigating the mean-flow structure of the interaction. Contours of Mach number and surface skin friciton coefficient were found that indicated highly varying levels of skin friction on the ramp. These areas were found to be tied to counter-rotating vortices that repeat in the spanwise direction of the flow. The cause of the growth of the vortices, according to the authors, may have been a results of the Görtler instability mechanism [15].

Görtler vortices are identified as pairs of counter-rotating vortices found on concave surfaces formed by centrifugal instabilities in high speed flow. They are cylindrical in shape,

and flow that is entrained in the vortex structure travels downstream in a corkscrew fashion [16]. The path of the flow and 3D structures of the Görtler vortices is shown in Figure 2.5.

Of course compression ramps are not concave in shape, but as Navarro-Martinez and Tutty [29] state when a high speed flow creates SWBLI in the corner of a compression ramp, the sharp corner is smoothed by the low velocity flow, and incoming air treats the structure as concave. This behavior is shown in Figure 2.6 from [29]. Navarro-Martinez and Tutty worked to understand the striation pattern of alternating high and low skin friction coefficients on a compression ramp behind a SWBLI.

They found that the reattachment line that is in the span wise direction on the ramp is made up of a series of alternating nodes and saddles. The nodes correspond to streaks of high skin friction, while the saddles sit directly ahead of and correspond to the regions of lower skin friction levels. Later in this current work, Görtler vortices will be identified in the flow field and the effect of the gap addition on these vortices revealed.

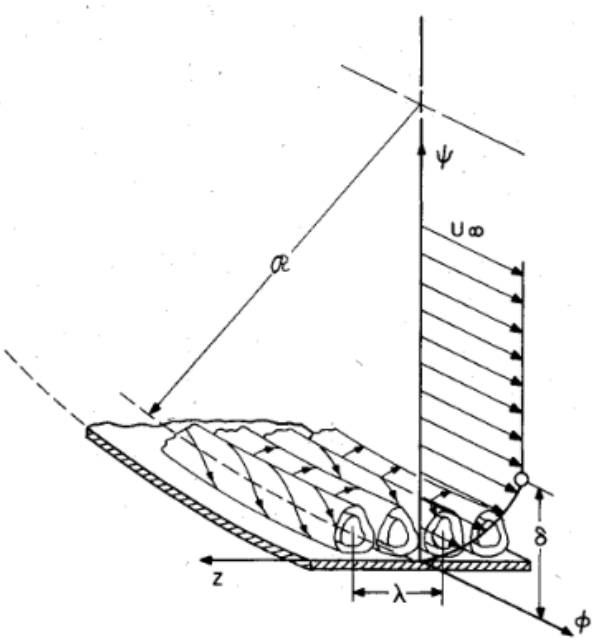

Figure 2.5: Vortex-like Disturbances in the Boundary-Layer Flow over a Concave Wall from [16].

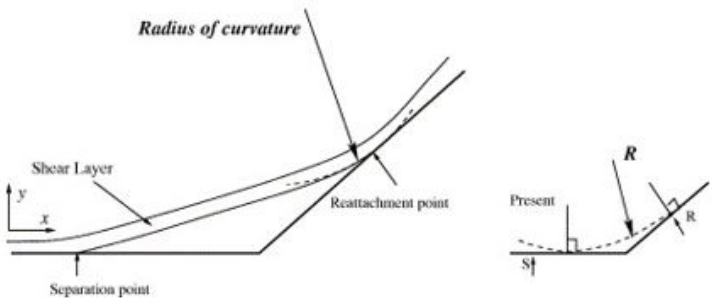

Figure 2.6: Planar Sketch of the Radius of Curvature from [29].

2.5 Gap Research

Over the years, various methods have been evaluated to mitigate the negative effects of SWBLI on aerodynamic bodies. These methods include micro-ramps and other vortex generators [30] [13] [25], suction [24] [20], and mass injection [35] [36]. Only one study was found that used a gap to reduce the size and effect of SWBLI, done by Mack et al. [22]. Their goal was to evaluate improvement of heat flux for hypersonic vehicles in stationary flow with multiple geometries. They tested 2D and 3D configurations for a compression ramp with an opened and closed gap. They found that with the closed gap a large separation bubble sat over the corner. The shock was induced at the site of separation. Then with the addition of the open gap, reverse flow led to a saddle point at the front of the ramp and a small vortex in the gap insulated the flow from going into the gap itself. They found reduced temperatures on the ramp with the addition of the gap, also. The temperature for the wall on the plate ahead of the corner reduced by 40%. The design used in the Mack et al. research is shown in Figure 2.7. This design is different from the current work as the gap at the corner was part of a long hole separating two large sections of forward structure with a flat plate at the top and back structure with ramp on top. The gap design that follows is much smaller and meets the free stream on the other side of a "wing." Despite the gap design, however, the behavior of the flow in response to the gap remains the same.

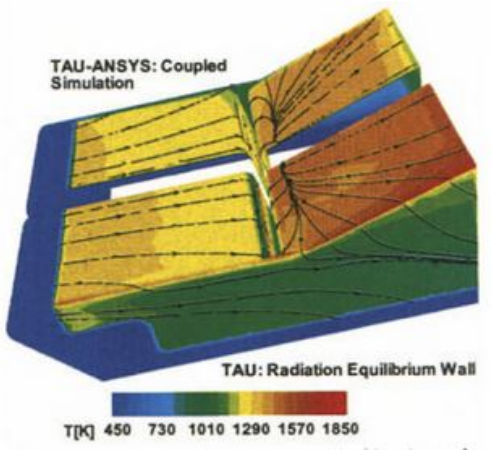

Figure 2.7: Supersonic Compression Ramp with SWBLI Mitigating Gap [22].

Chapter 3

Half Domain Case

A simulation was created to mimic the setup and results of the Geisking et al. [19] work for a 24° compression ramp in Mach 2.84 flow. The intent of this process was to learn the appropriate ways to design a geometry, create a mesh, and set boundary and flow conditions for a SWBLI at a compression ramp. After duplicating the results of this research, the methods were carried forward into the gap study. ANSYS Fluent [5] was used for all simulations and mesh generation was performed using Pointwise. Post-processing was performed with Paraview.

3.1 Background

3.1.1 Setup

The simulations in [19] are representative of a compression ramp attached to the floor of wind tunnel. In the past, 2D simulations have been used in the study of SWBLI at a compression ramp. For the simulations in the present work only 3D was used because there are characteristics of the flow that appear only in 3D that are relevant for the study of Gap vs. No Gap cases. The five sided geometry used in the simulation in [19] extends from -0.35 m to 0 m on a flat plate in the direction of flow (X). It extends 0.125 m in direction normal to the bottom wall (Y). The intersection of the flat plate and the ramp is located at X = 0 m. The ramp is a length of 0.175 m in the direction of flow and rotated 24° about the Z

Table 3.1: Freestream and Boundary-Layer Properties Mach 3

Case	M_∞	δ_0, mm	$U_\infty, m/s$	Re_δ	P_0, Pa	T_0, K	C_f
Gieseking et al.[19]	2.84	25	570	$1.69 \cdot 10^6$	$6.8 \cdot 10^5$	260	$1.00 \cdot 10^3$

axis at the corner. In the span-wise direction the mesh extends from -0.075 m to 0.075 m. The mesh spacing from [19] was duplicated giving a minimum Y+ of 0.99 in the boundary layer and the first cell off the wall was located at $5 \cdot 10^{-6}$ m normal to the wall. These sizing and meshing parameters and the following boundary conditions were replicated from [19] to produce a mesh which will from here on be referred to as the Half Domain case. Chapter 4 will introduce the Full Domain cases.

Table 3.1 lists the provided freestream and boundary layer properties of this calculation. The static temperature, T, and static pressure, P, were calculated with the isentropic relations shown in Equations 3.1 and 3.2, from [2], using the total pressure, P_0, the total temperature, T_0, and the freestream Mach number, M_∞. The specific heat ratio, γ , was 1.4. T was found to be 99.5 K and P, 235.75 kPa.

$$T = \frac{T_0}{1 + \frac{\gamma - 1}{2} M^2} \tag{3.1}$$

$$P = \frac{P_0}{1 + \frac{\gamma - 1}{2} M^2} \tag{3.2}$$

3.1.2 Boundary Layer

Special care was taken to ensure a boundary layer height of 0.025 m as specified in Table 3.1. An initial process was investigated that involved creating a parabolic shaped boundary-layer profile for velocity and imposing the profile on the inlet. However, this method was determined to be insufficient, because the temperature of the inlet profile was left untouched, and the shape of the boundary layer profile was based on the (1/7)th power velocity profile law [27]. Instead the method for boundary layer growth from an ANSYS tutorial by A. Gerasimov was used [18]. Using Pointwise, the inlet face from the existing geometry was extruded three times in the X direction by a distance equal to the largest cell edge length

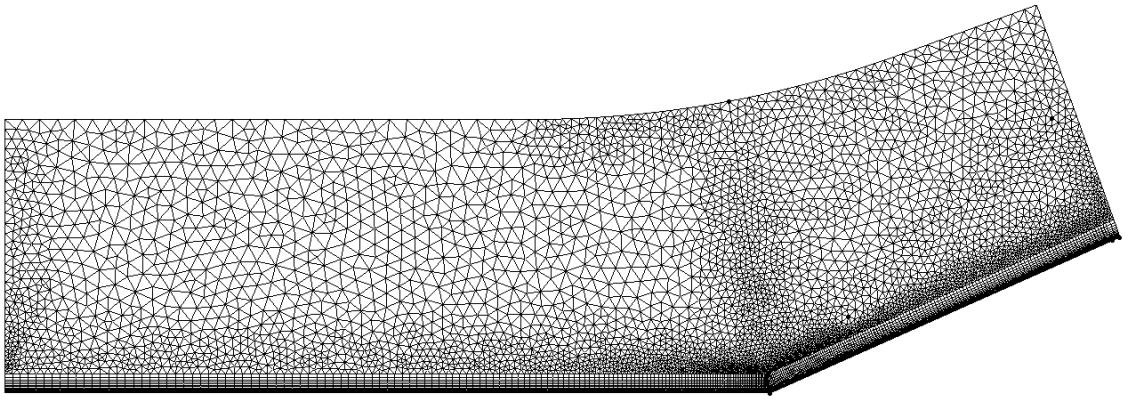

Figure 3.1: Half Domain Mesh

at the inlet face. In this case the largest cell edge length was 0.00156 m. The total length in X for the extrusion block was 0.00468 m. The extrusion created a six-sided, 3D, structured mesh. The original fluid zone was deleted, and the extrusion mesh was saved. Next, inside Fluent, the boundary conditions were set for the new geometry. The bottom surface was set as a wall. The top face and side wall faces were set as symmetry planes. The geometry is shown in Figure 3.2 with a focus on the mesh sizing for the extrusion distance. Finally, the inlet and outlet of this new domain were set as periodic boundary conditions.

Translational periodic conditions matched two defined faces and superimposed the results calculated on the outlet face onto the inlet face. As the simulation proceeded, this process was repeated at every calculation. Periodic conditions were set in Fluent with a mass flow rate on the inlet/outlet pair, $\dot{m}$, of 87.2 kg·m^2/s, calculated from Equation 3.3.

$$\dot{m} = \rho U_\infty A \tag{3.3}$$

The area of the inlet, A, was 0.01875 m^2 and the freestream velocity and density were set as 570 m/s and 8.26 kg/m^3. The prescribed mass flow rate at the inlet forced air through the flow domain and as air passed over the bottom wall, the boundary layer grew. After each

step in the solution, the boundary-layer height at the outlet was then matched at the inlet, and the boundary layer continued to grow from that point. This process was continued until the boundary-layer reached the height specified in [19], 0.025 m. This height was verified in Paraview by creating a contour of velocity set to 99%, of the freestream velocity. The highest contour surface marked the point where the velocity boundary layer profile ends and the flow no longer is affected by the wall. Figure 3.3a shows the contour of velocity magnitude at 99% of the freestream velocity, indicating a fully developed boundary layer with a height of 0.025 m. Figure 3.3b shows the effect of the wall on temperature. Figure 3.4 shows how the velocity changes with distance from the wall. The boundary layer was developed in this manner to create a profile with both velocity and temperature factors, and one that is true to the initial temperature and pressure constraints of the full simulation. After development, the profile on the outlet of the domain was saved for use in the full SWBLI domain.

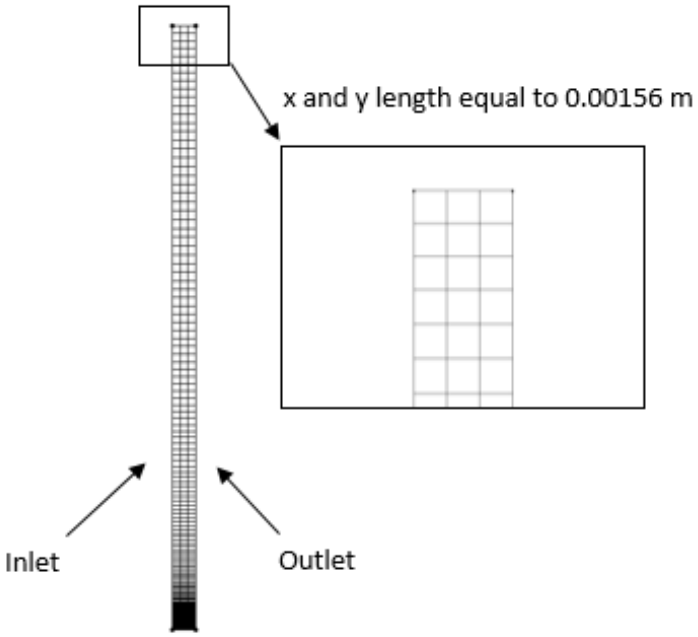

Figure 3.2: Boundary Layer Recycling Extrusion Block

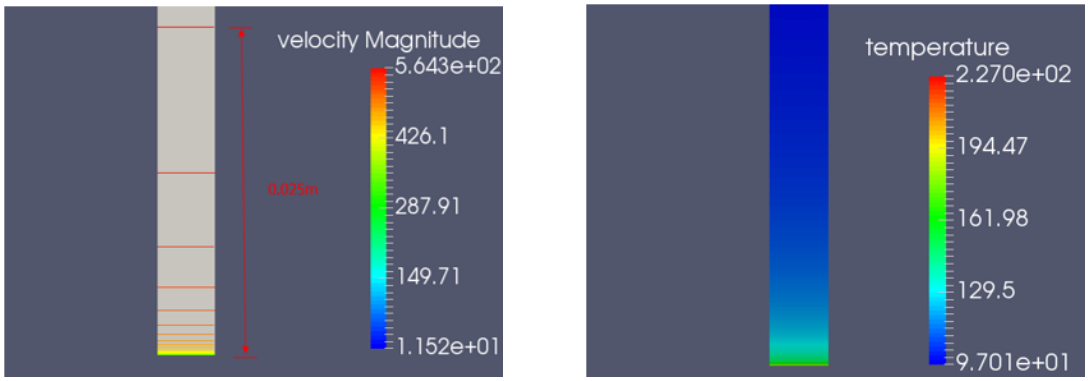

(a) Velocity Magnitude Contour **(b)** Temperature Contour

Figure 3.3: Boundary-Layer Profile Generator Results

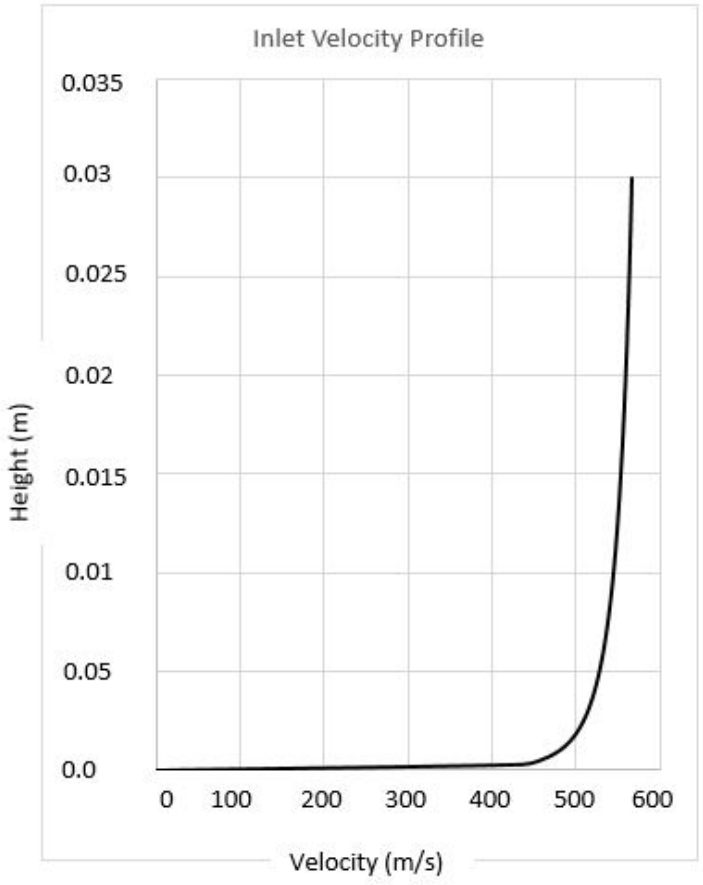

Figure 3.4: Boundary-Layer Velocity Profile

3.2 Turbulence Model Choice and Methodology

Gieseking et al. [19] used a hybrid Reynolds Averaged Navier Stokes/Large Eddy Simulation (RANS/LES) solver that was developed in-house. For the RANS component, they used a modified Menter BSL model [28] . The RANS portion of the solver was developed to intentionally switch to LES as the attached boundary-layer makes its transition from logarithmic structure to its wake like response. In Figure 2.3, this position is specified as the "outer layer." They used a recycling method to develop their boundary-layer and then reached convergence with a precursor steady-state RANS simulation before switching to the transient hybrid RANS/LES simulation. This procedure allowed for the transient simulation to start with an already developed flow in an effort to cut down on the expense in time and computational power required to run a hybrid RANS/LES code from initialization. The authors were predominately interested in the behavior of the SWBLI over time and were able to perceive the large, low frequency oscillation of the shock and recirculation region that is characteristic of the SWBLI phenomenon at a compression corner. They found an average frequency of the motion of the shock to be 0.31 kHz.

The initial scope of this research included performing simulations using a type of hybrid RANS/LES solver known as Detached Eddy Simulation (DES) to track the shock and recirculation region motion over time on cases with and without a ramp foot gap. However, this level of computation required resources and time outside of those available. The constraint forced the scope of study to remain firmly steady-state. Non-transient simulations on SWBLI will not capture the oscillations and unsteadiness that is a large part of current study, but there is still a wealth of information that can be garnered from steady-state data. The results of steady-state simulations herein can be used as a precursor of study for other experiments and tests. In this research, the study of how the addition of a gap at the foot of a compression corner will mitigate the effects of SWBLI (particularly in regard to pressure and thermal loading) can help give insight into geometry design, material selection, thermal protection system design, and internal component selection and placement. Also, the use of steady-state runs using only a RANS model allowed for more test cases to be run and more avenues of study to be explored in the same amount of time as the DES study.

The inability to perform hybrid RANS/LES simulations allowed the selection of RANS turbulence model to become more open and more important. The options were numerous but the results of a paper by Acquaye [1] were very beneficial in narrowing the field. In that study, three turbulence models were tested in a 2D, steady state simulation of a compression ramp with ramp angles of 8 ° and 16 °. The goal was to compare the effectiveness of three RANS codes against experimental data. The three codes were: Spalart-Allmaras (SA), Shear Stress Transport $k-\omega$ ($k-\omega$ SST), and Wray-Agarwal (WA). All three models performed well when predicting surface pressure but performed poorly when predicting skin friction coefficient for the 8° simulation. During the higher angle ramp test of 16°, the $k-\omega$ SST predicted a sudden increase in pressure much farther ahead of the corner than experimental results suggested. This was most likely due to over-predicting flow separation. The SA and WA performed well here and matched the experimental results much more closely. The WA fell short when comparing the results of skin friction coefficient to experimental data. Here, too, the $k-\omega$ SST over-predicted separation point. Finally, the Spalart-Allmaras model was chosen because the results matched the experimental data well for pressure, matched better than WA for skin friction, and did not display the same over-prediction tendencies as $k-\omega$ SST.

Spalart-Allmaras is a one-equation turbulence model that solves a modeled transport equation for the kinematic eddy viscosity [4]. It requires meshes that are properly resolved with $y^+ = 1$. It was developed for use in aerodynamic applications with wall-bounded flows [34]. Also, it has been shown to give good results for boundary layers subjected to adverse pressure gradients like the ones encountered in SWBLI study [4].

3.2.1 Solving and Results

The 3D mesh, shown in Figure 3.5 was imported to Fluent and the boundary conditions were set from Table 3.1, the static temperature, and the static pressure. The SA model was used for turbulence. The generated boundary layer profile was imported and applied to the inlet face. The simulation was run to convergence. Convergence for these simulations gave residuals below 1e-4. Also, mass flow monitors were set on the inlet and outlet, and at convergence the values for mass in and mass out were equal. Figure 3.6b shows the contour of temperature compared to the temperature contour from [19] shown in Figure

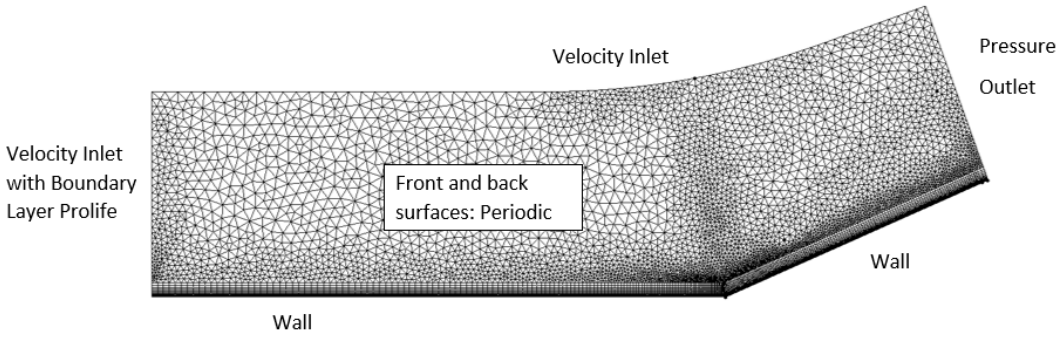

(a) Side View

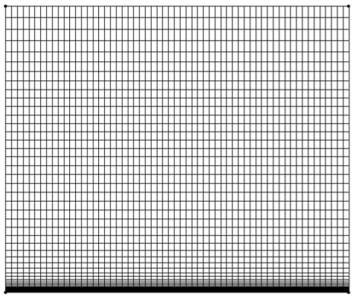

(b) Inlet

Figure 3.5: Half Domain Mesh with Boundary Conditions

3.6a. Graphically, it can be seen that the two are very similar. The shape and size of the recirculation region is consistent, and so too is the shockline.

In Chapter 2, it was stated that compression waves emanate from the low velocity region behind the separation point and coalesce into a shockwave farther and higher into the flow. This phenomenon can be seen in the temperature contour above the separation point as a lightly colored region that forms a straight shockline and meets the recompression wake.

The interaction in the corner of the shockwave and the boundary layer is three-dimensional. The streamlines in Figure 3.7 show the tendency of the recirculation region in the No Gap case to vary in size and shape along the span-wise direction. In this research streamlines refer to the mean flow as calculated by the RANS-type equations in the SA turbulence model. One of the most important references of a SWBLI study, the point of separation, also varied in the span-wise direction.This is shown by the uneven separation line indicated in Figure 3.7 Therefore, for plotted comparison data to be representative of the entire width of the domain, it was essential that the flow be span-wise averaged along the

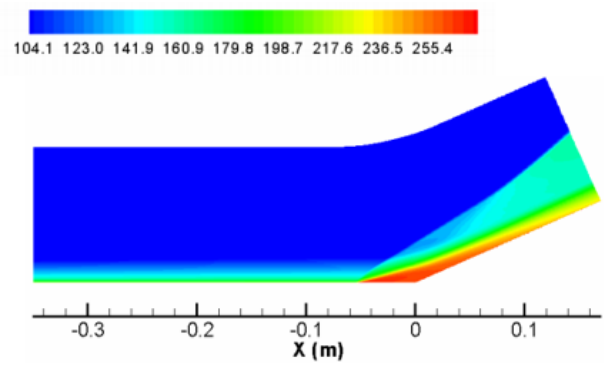

(a) Contour from [19].

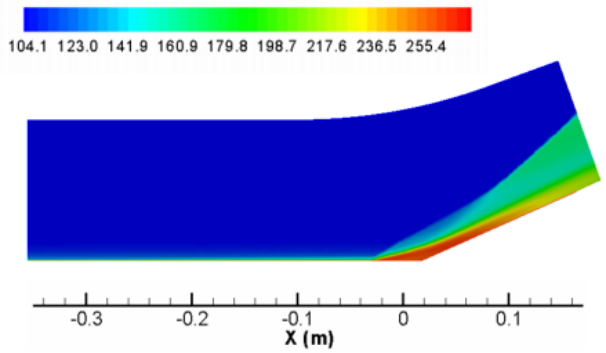

(b) Half Domain

Figure 3.6: Comparison of Span-averaged Temperature Contours

Z axis. In Paraview, slices were taken normal to the Z axis at every cell along the axis and the cell data associated with each slice was averaged. This same procedure was performed in [19].

To understand how the SWBLI affects the flat plate and ramp, surface data had to be extracted. Surface data was pulled from the simulation in Paraview along the Z axis for every cell in that direction and averaged to give the aggregate conditions of the flow along the walls. Figure 3.8 shows the surface pressure distribution on the flat plate and ramp plotted against the results from [19] and data from [10] and [32], the two sources of data to which Gieseking et al. compared their data P_w is the surface pressure, and is normalized by P_{inf}, the freestream pressure. This figure shows where the separation point occurs for the Half Domain case, specified in the figure as "Spalart Allmaras," and how that compares to the other simulations. The point occurs at X = −6.4 cm for Choi [10], at X =−4.8 cm for Settles et al. [32], and at X = −5.5 cm for Gieseking et al. [19], where X = 0 is at the

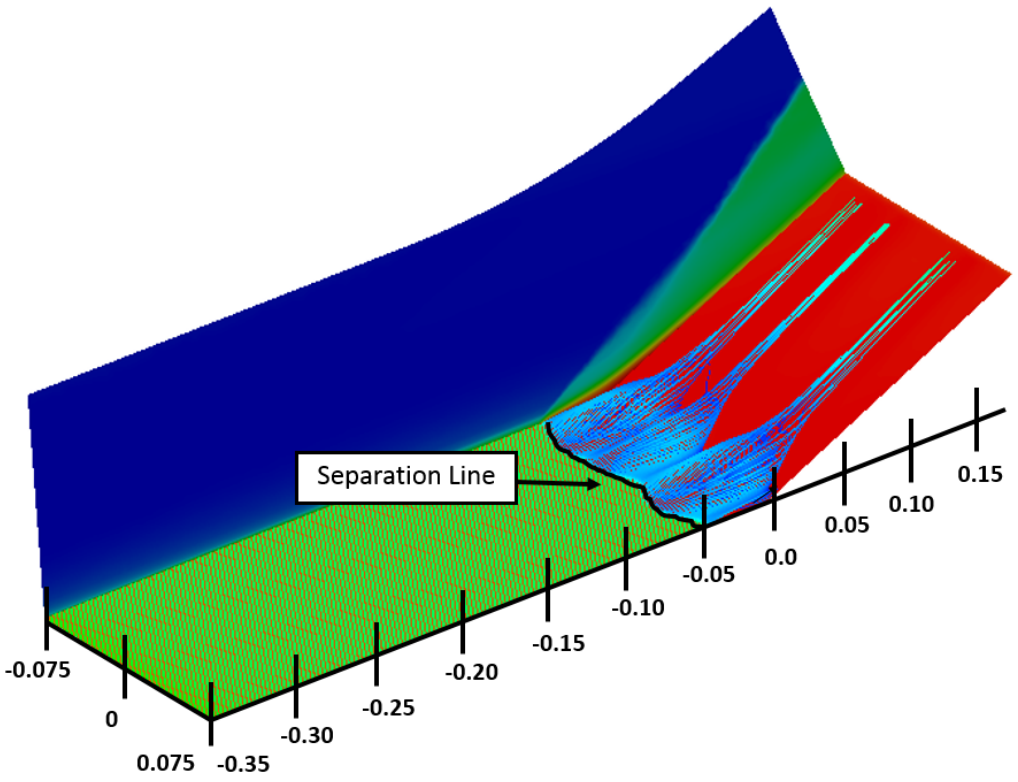

Figure 3.7: Streamlines Near Wall of Half Domain

corner. The separation point calculated in the Half Domain case is located at X = −4.9 cm, which sits safely between the other three.

In the upper region of the ramp, beyond approximately X = 0.075 m, the pressure is over-estimated compared to the other plots, but along the flat plate and the through the interaction region the data are well-matched. The Half Domain case had an average error of 6.7% with the Gieseking [19], 3.9% with Choi [10] and 3.8% with Settles [32].

The results show that for generating and comparing steady state, span averaged results, the SA RANS turbulence model worked. The size and shape of the shock and interaction region was very close to Gieseking et al., and the surface pressure distribution matched closely to the other existing data. Recreating this simulation provided a baseline case and a reference point for the rest of the subsequent research. The geometry, mesh sizing, boundary and flow conditions, and boundary-layer inlet profile generation method were carried into the next segment of this research.

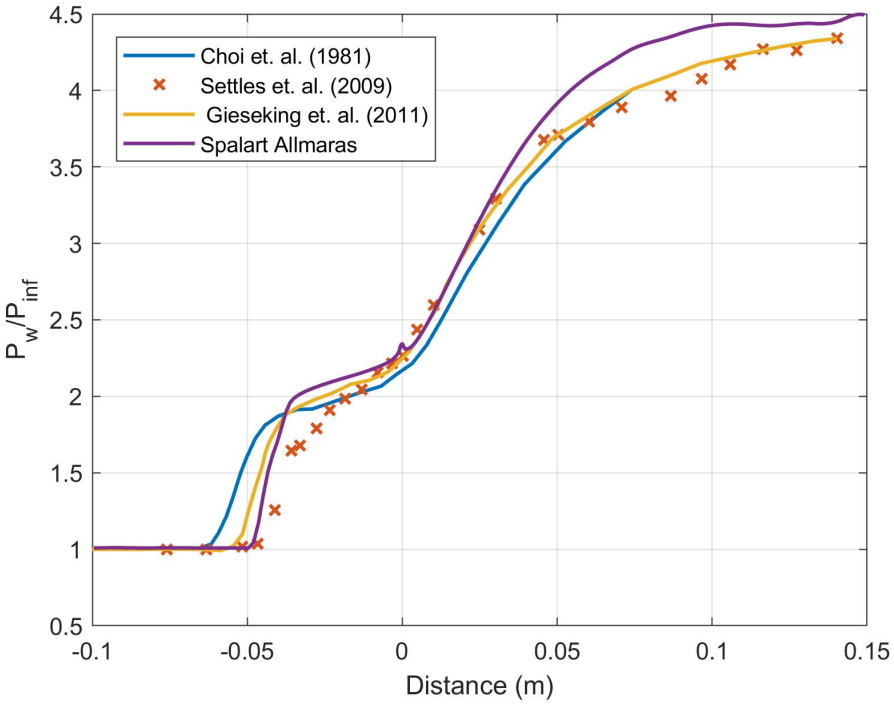

Figure 3.8: Surface Pressure Distributions

Chapter 4

Full-Domain Case

The hypothesis of this research was that adding a gap to the foot of a compression ramp corner in supersonic flow would help to mitigate the negative effects of SWBLI. After using the previous case to understand how SWBLI works and to understand how to set up a simulation to achieve separation, reattachment, and a recirculation region at the corner, a gap had to be implemented into the geometry. The Half Domain case was so named because there was only airflow on top of the flat plate and the ramp. To fully realize the effects of a gap through a surface, a lower section of the geometry had to be created. The lower half consisted of the bottom of the flat plate and the underside of the ramp. The total shape of the structure is reminiscent of a wing or stabilizer with a control surface in full deflection but can be representative of any aerodynamic structure with a compression ramp on top of a flat plate and an expansion corner below it. The thickness, t, was chosen to be 0.00635 m or 0.25 in. This geometry is called the Full Domain case. The case comes in two variants: No Gap and Gap cases.

4.1 Setup

Shape and size were important design features for the gap, and additional investigations into other options could be an interesting topic for follow-up work in the future. For this research, the gap design was chosen as a ball and socket type connection instead of a straight channel. The curved shape of the hole was selected to allow more room for recirculation to

occur. As mentioned in Chapter 2, a similar gap shape was created in [22]. It was found that the size and shape selected allowed a recirculation region to form that kept much of the incoming air from entering the gap.

To determine the appropriate size for the gap, a number of preliminary runs were performed with a simpler geometry and flow at Mach 3. The gap width, w, was non-dimensionalized by t, and widths of $w = 0.2$, 0.3, 0.4, and 0.5 were tested. These gaps are shown in Figure 4.1 with streamlines showing the interaction of air in the boundary layer with the recirculation region. It was found that widths of 0.2 and 0.3 were too small for the recirculation region to fully form at a Mach number of 3. At a width of 0.5, the recirculation region became fully formed but the gap was deemed to be too large. With this 0.5 width gap the boundary layer at the front of the ramp was larger than the others, and the low velocity region between the flat plate and ramp began to stretch outside the confines of the gap on the underside of the ramp. A width of w = 0.4 was chosen. This size is a compromise between the others. It was found large enough for a recirculation region to easily form but not to large that it woukld encroach onto the ramp.

Next, using the chosen shape and size design, the Full Domain No Gap case was edited to create the Full Domain Gap case. The analysis of these two cases served as the first section of the study of the gap's effectiveness.

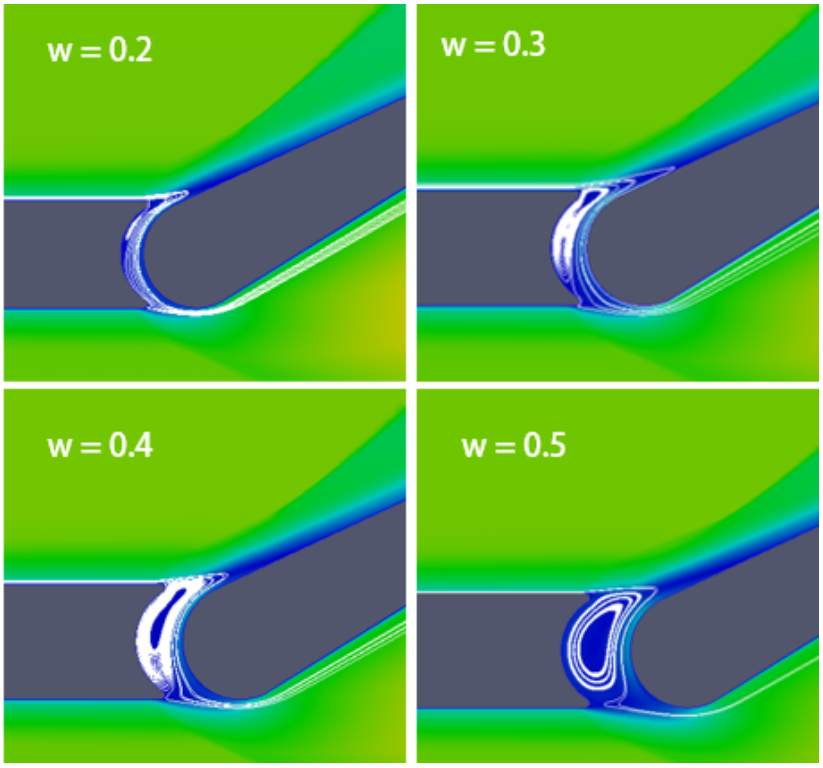

Figure 4.1: Gap Design Options Showing Streamlines Through Gap

The boundary conditions were the same as the Half Domain case, and the inlet conditions were used for both the upper and lower halves of the Full Domain. To replicate the boundary layer created on the upper flat plate in the Half Domain case, the procedure described in Chapter 3 was repeated with both halves of the domain. Both inlets in front of the flat plates were extruded and the faces were set as translational periodic boundary conditions to grow the boundary layer to 0.025 m. The result of boundary layer generator for the upper and lower inlets is shown in Figure 4.3. Finally, both the No Gap and Gap cases were run to convergence. Figure 4.2 shows an example of what the ANSYS Fluent residuals look like for these simulations.

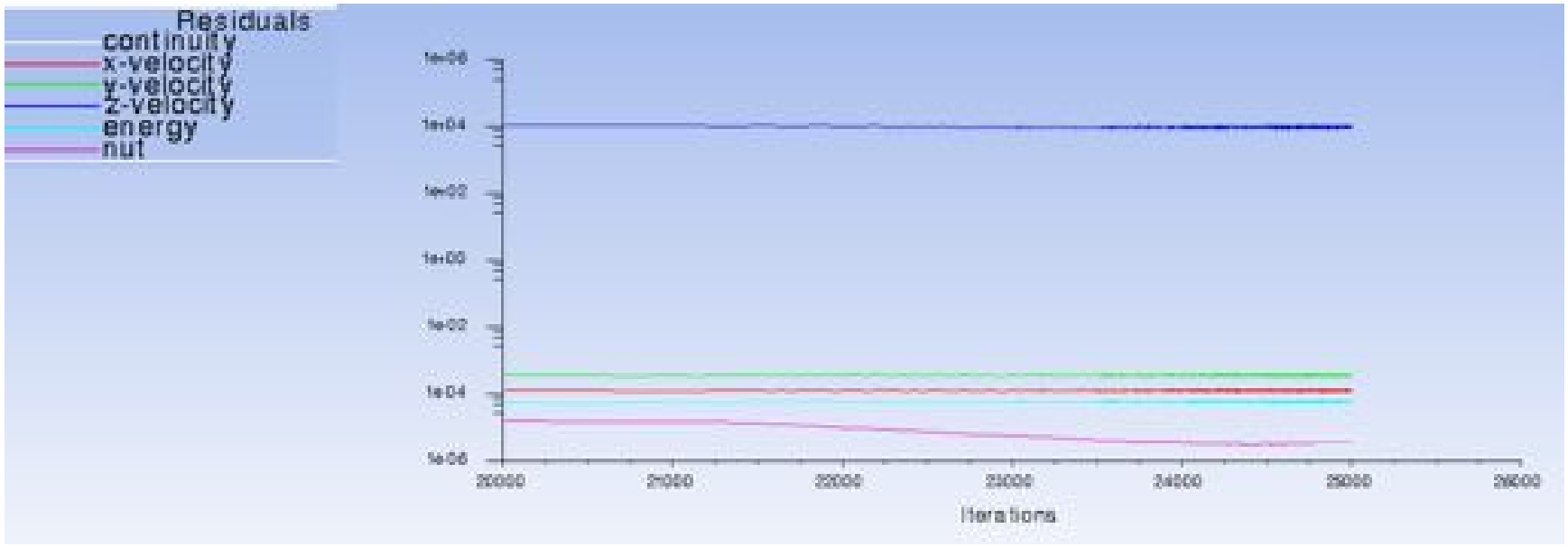

Figure 4.2: Fluent Residuals for Full Domain Case

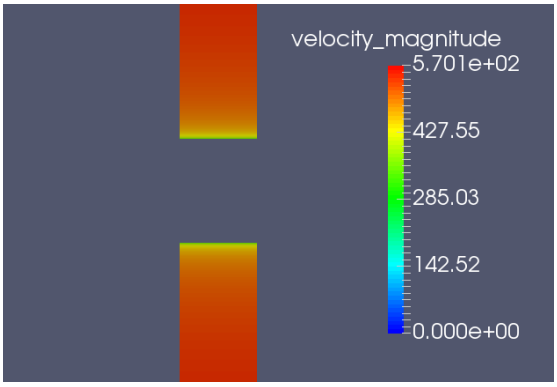

(a) Velocity Magnitude Contour of Profile

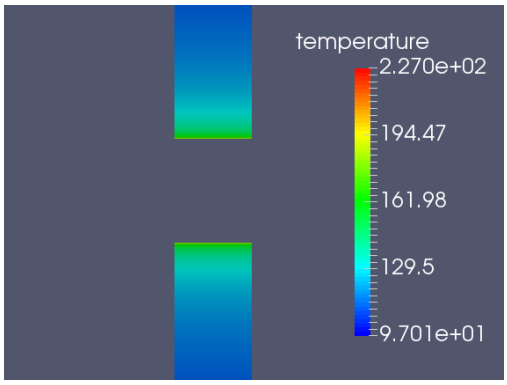

(b) Temperature Contour of Profile

Figure 4.3: Full Domain Upper and Lower Inlet Boundary Layer Profiles

4.2 Results

4.2.1 Contours and Surface Plots

A comparison of the two cases shows considerable differences. Figures 4.4 and 4.6 show the result of the gap on the flow with contours of Mach number and temperature. The most obvious physical feature change is the location of the recirculation region. Close-up images of the interaction region in Figure 4.5 show that in the No Gap case the standard SWBLI region appears in the corner as to be expected. In the Gap case, however, the SWBLI region disappears. There is no effect of lower velocity flow or temperatures displayed on the flat plate section of the structure. The temperature on the flat plate stays constant all the way to the gap. Also, for the No Gap case, the shockline has two distinct sections. The lower section of the shock is formed by the coalescence of compression waves emanating from the low velocity recirculation region ahead of the corner. This section meets the recompression shockline at a point half-way up the ramp. In the Gap case, the shock is a straight line impinging directly from the corner of the ramp. Overall, the low velocity, recirculating flow region in corner the No Gap case is not present on the Gap Case flat plate whatsoever.

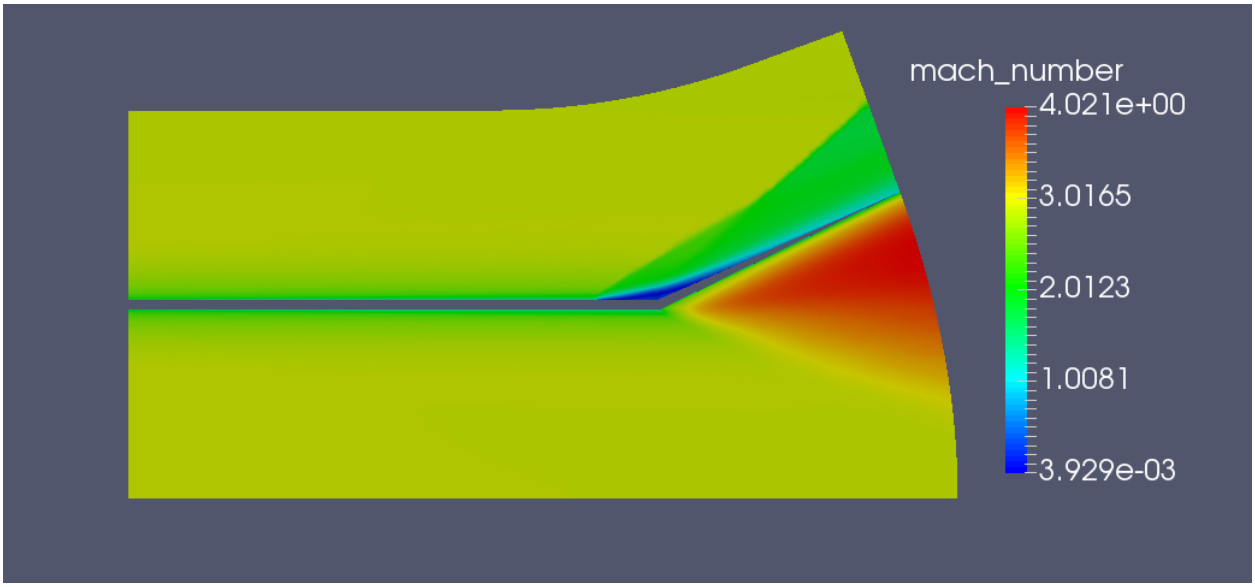

(a) No Gap Case

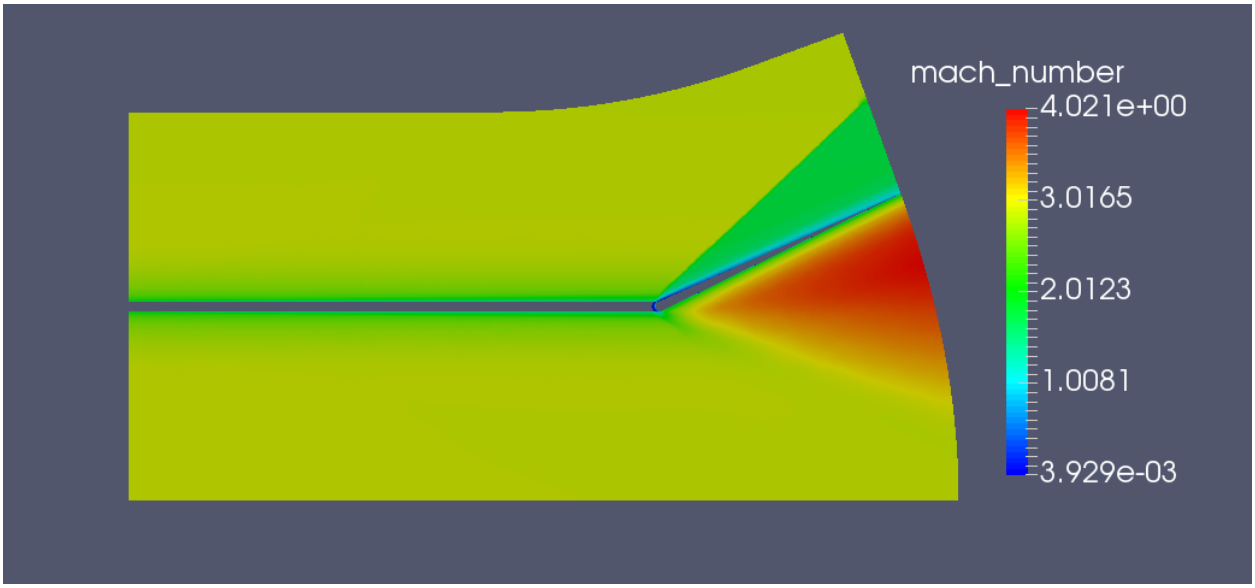

(b) Gap Case

Figure 4.4: Full Domain Mach Number Contours

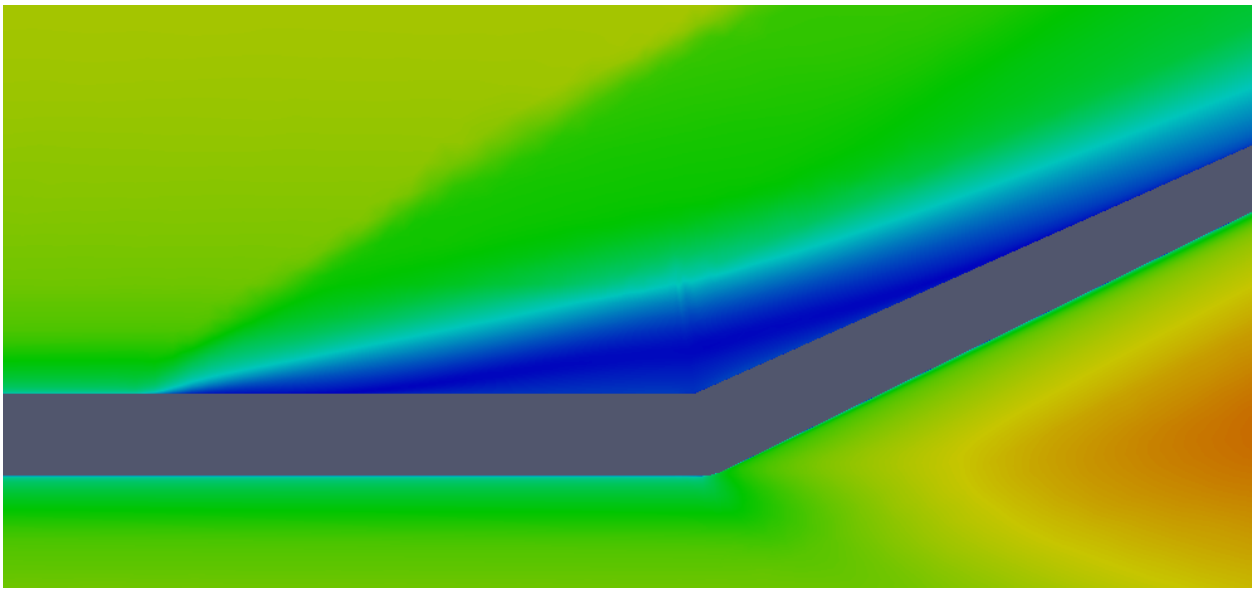

(a) No Gap Case

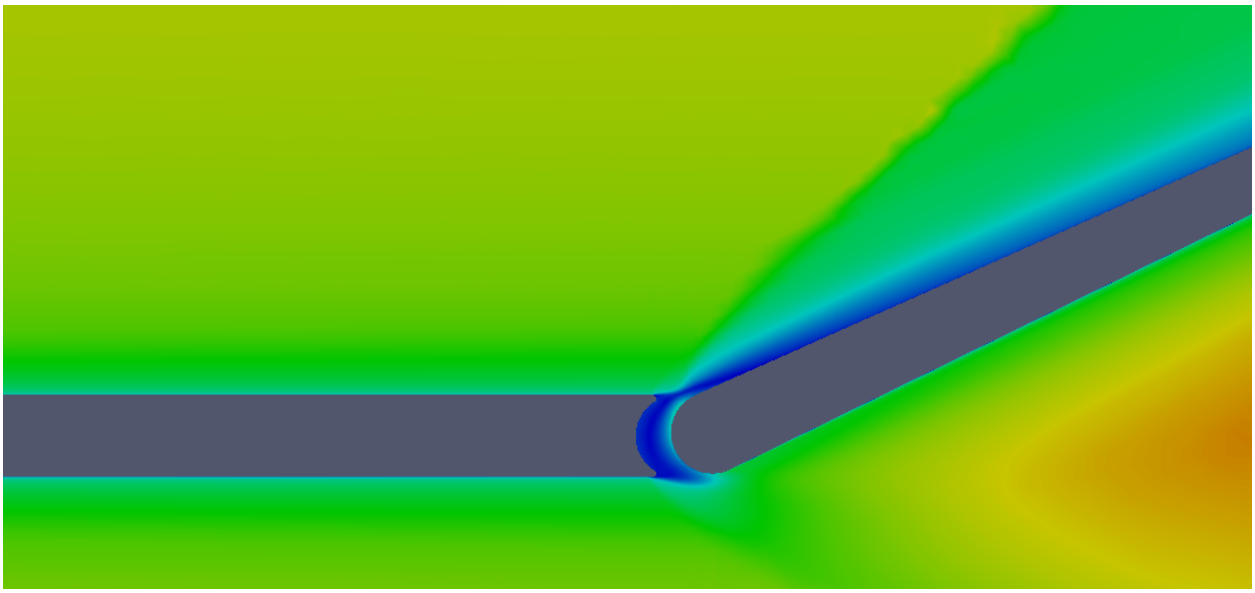

(b) Gap Case

Figure 4.5: Full Domain Mach Number Contours Close-up

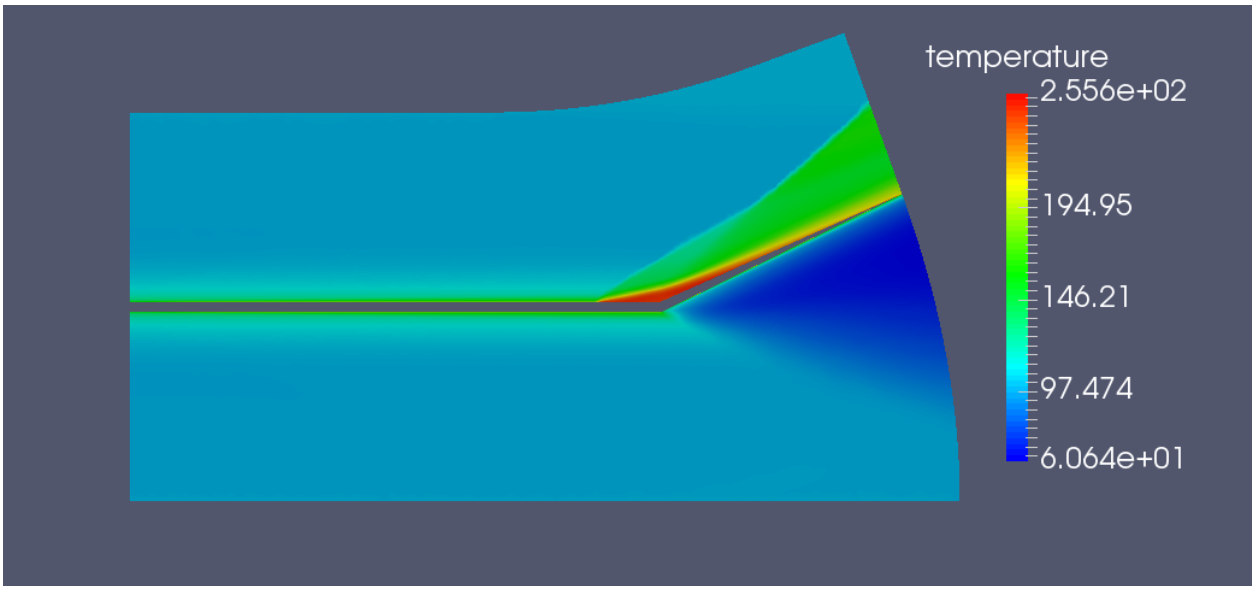

(a) No Gap Case

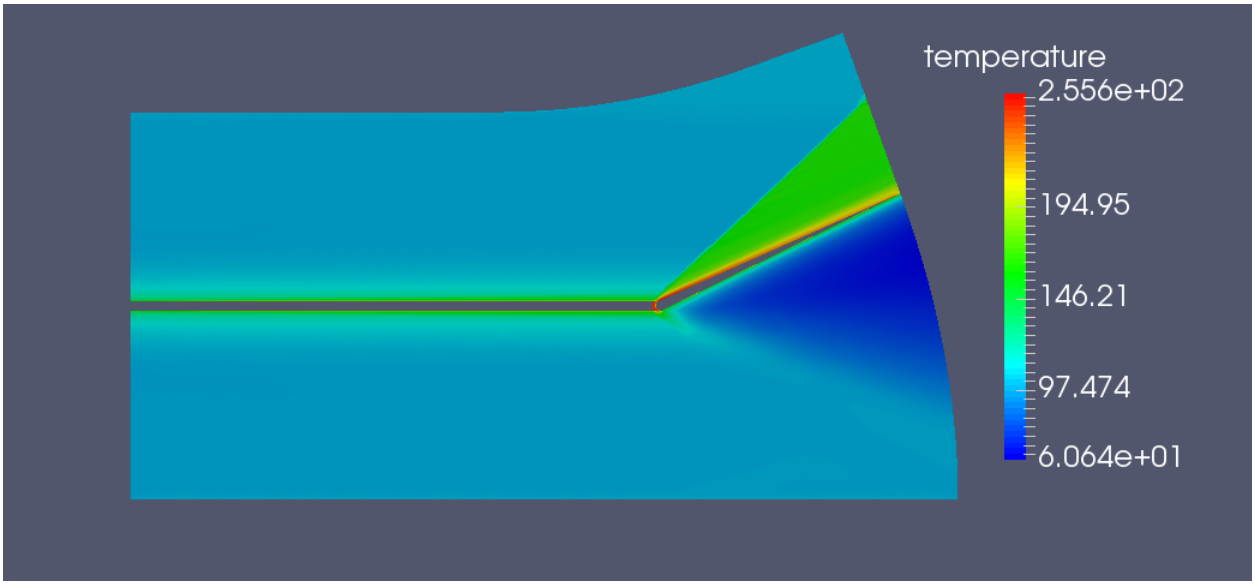

(b) Gap Case

Figure 4.6: Full Domain Temperature (K) Contours

The detrimental effects of SWBLI are commonly attributed to pressure loading and thermal effects. To understand exactly what the effect of the gap is on the structure, wall data for pressure, temperature, and surface skin friction coefficient were collected. As in the previous Half Domain case, the Full Domain simulations were run in 3D. To analyze overall effect, while accounting for variance in the span wise direction, averaging was performed. Slices of the domain were taken at every cell location in the Z direction and the surface data on the upper flat plate and upper ramp at theses slices were saved and then averaged.

A plot of surface pressure distribution normalized by the free stream static pressure, 235750 Pa, is shown in Figure 4.7. The plot shows that adding the gap removes all of the pressure on the flat plate section ahead of the corner that is normally present. Past the corner, there is a very sharp spike in the pressure for the Gap case, and the pressure level surpasses that of the No Gap case for a small section of the ramp. Both cases begin to experience similar pressure loading at a distance of 0.1 m up the ramp, however. On the flat plate there is a 29.7% decrease in pressure, and on the ramp there is an increase in pressure of 12.7% when the gap was added.

To analyze overall effect of pressure loading on the surface, an integral of the curves was used. The total pressure loading was 1.69 kPa for the No Gap case and 1.71 kPa for the Gap case. As there is no pressure loading on the flat plate with the Gap case, the entirety of the loading was on the ramp. Under these conditions the No Gap case actually performed slightly better with 1.2% less loading across the structure.

Next, Figure 4.8 shows a plot of surface temperature distributions. The plot shows that adding the gap allows the temperature on the flat plate to stay constant all the way to the corner, while there is an increase in temperature inside the recirculation region for the case without the gap. The maximum temperature experienced on the surface in each case is 248.9 K for Gap and 248.4 K for No Gap. The average temperature for the No Gap case is 244.7 K and 242.1 K for the Gap case. So, while the maximum is nearly equivalent, it can be seen that the average temperature along the surface is lower when the gap is added.

The skin friction coefficient on the surface is another variable that was determined to be relevenant for comparison. The effect of the gap addition is shown in Figure 4.9. This coefficient expresses a relationship between friction force and shearing stress and is a

component of the overall drag coefficient. Similar to temperature, the average skin friction coefficient on the surface is slightly higher for the Gap case by 1.5%, but the maximum is higher for the Gap case. The most obvious, contrasting feature in the comparison is how the location of low friction changes. In the No Gap case, the area of lowest friction is in the recirculation region on the flat plate. The friction increases with distance up the ramp. In the Gap case, the friction stays constant on the flat plate, instead of decreasing. On the ramp, however, friction does not increase nearly as sharply or reach the same high values as the No Gap case. By the top of the ramp the skin friction coefficient is over 100% higher for the No Gap case compared to the Gap case.

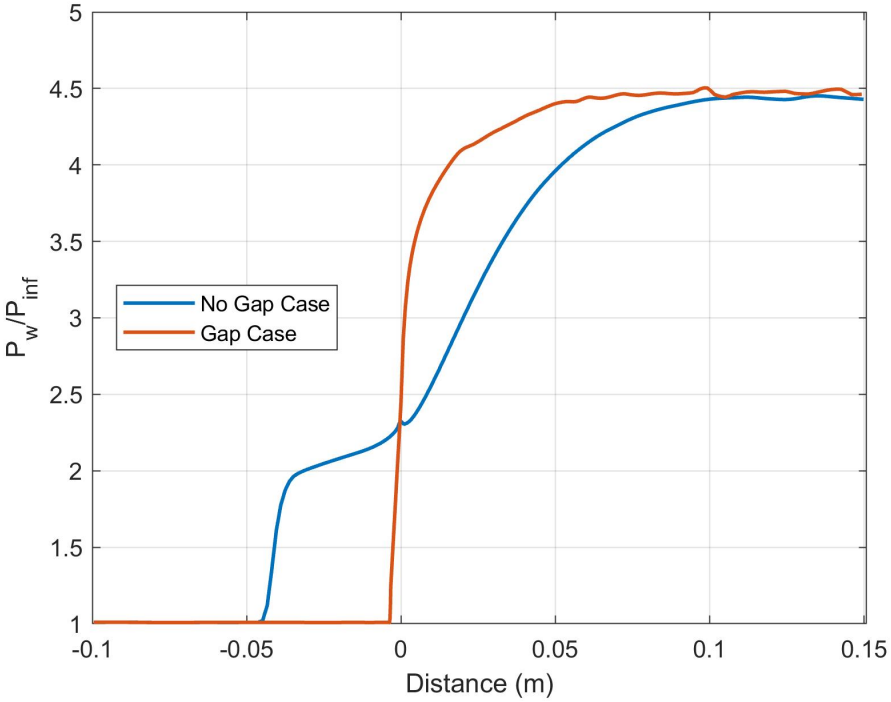

Figure 4.7: Surface Pressure Distribution

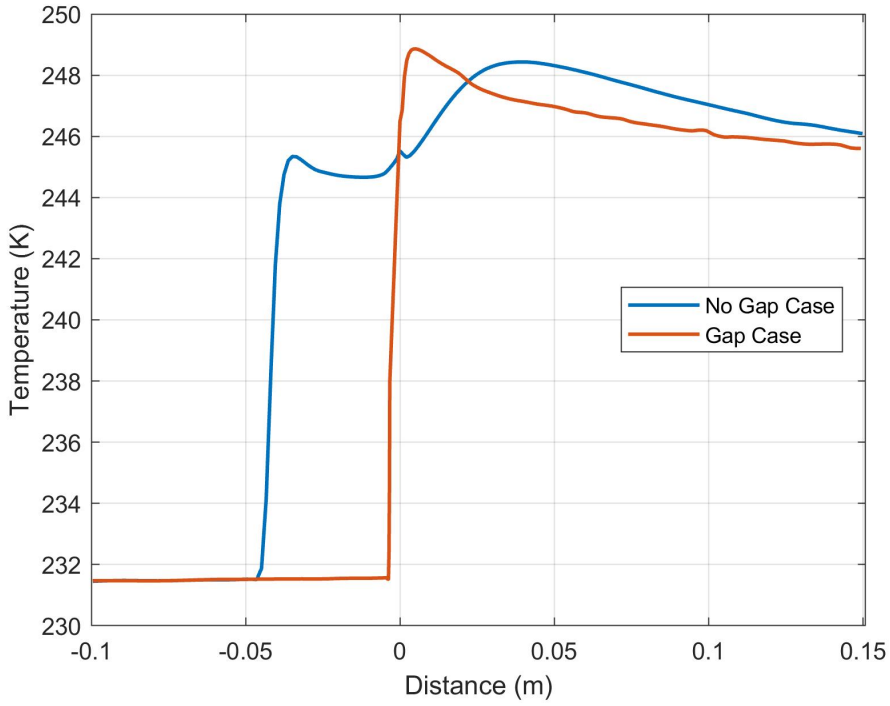

Figure 4.8: Surface Temperature Distribution

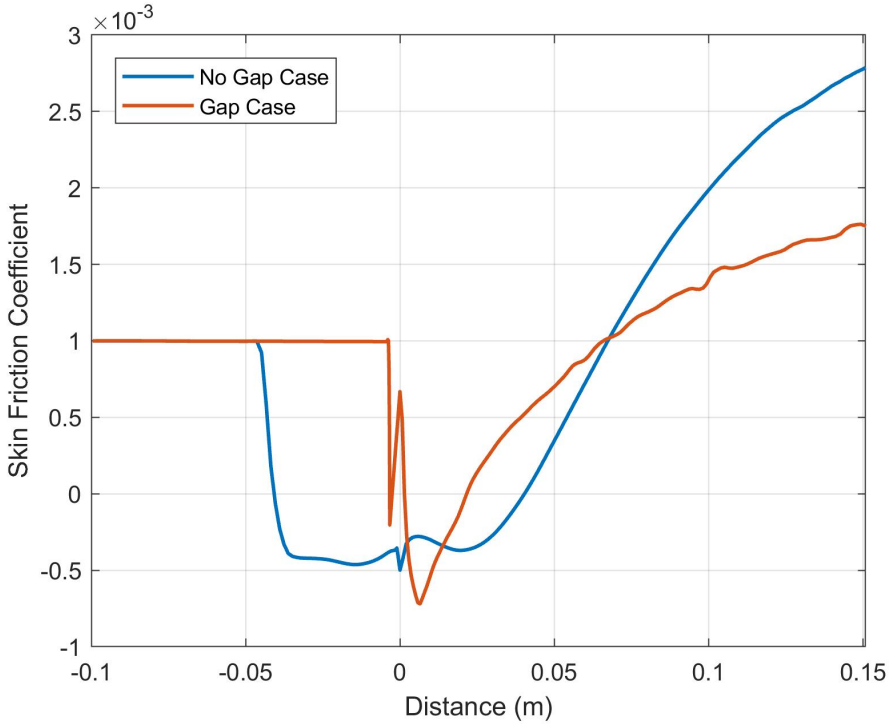

Figure 4.9: Surface Skin Friction Coefficient Distribution

4.2.2 Hinge Moment

It was found that the the overall pressure on the upper surfaces of the wing is slightly higher in the Gap case. However, the location distribution of pressure across the surfaces changes significantly. In the Gap case there is a very low amount of pressure applied to the flat plate and more applied to the ramp. The No Gap case contains reverse effects. This change in loading prompted a study of how the addition of a gap would change the hinge moment of the wing.

To find the hinge moment of the surface before and after the gap addition, the solution was brought into Paraview. Here, the surface normals were calculated for each surface. Pressure components in the Y direction were expressed as lift, and components in the X direction were expressed as drag. The hinge point used was located at (0, -0.003175), a point halfway through the thickness below the corner. Moments were calculated by gathering the lift and drag values for each surface and multiplying by the distance in x and y each surface's midpoint to the hinge point. After summing all the moments for the Gap and No Gap cases it was found that the No Gap case produced a hinge moment of 1773.7 N*m while the Gap case produced a higher moment of 1977.5 N*m. This is an increase of 11.5% and can be mostly attributed to the shift in pressure distribution from the flat plate to the ramp. Figure 4.10 breaks the geometry into upper and lower halves and shows the No Gap case with pressure normal to the surface. Figure 4.11 does the same for the Gap case and does a good job showing how little influence the gap has on the underside of the ramp. In fact, the lower ramp surfaces experienced nearly identical pressure loading at 325.7 N/m and 331.4 N/m, for the No Gap and Gap cases, respectively.

4.2.3 Streamlines

As Floryan noted in [16] the flow in the recirculation region of a compression ramp SWBLI has a tendency to form coherent structures. In Figure 4.12a a top view of the flat plate and ramp is shown for both Gap and No Gap cases. Streamlines were initiated at the front of the domain, 0.001 m above the surface. In the No Gap case, incoming air stayed straight along the flat plate but as it approached the corner the air entered recirculation structures

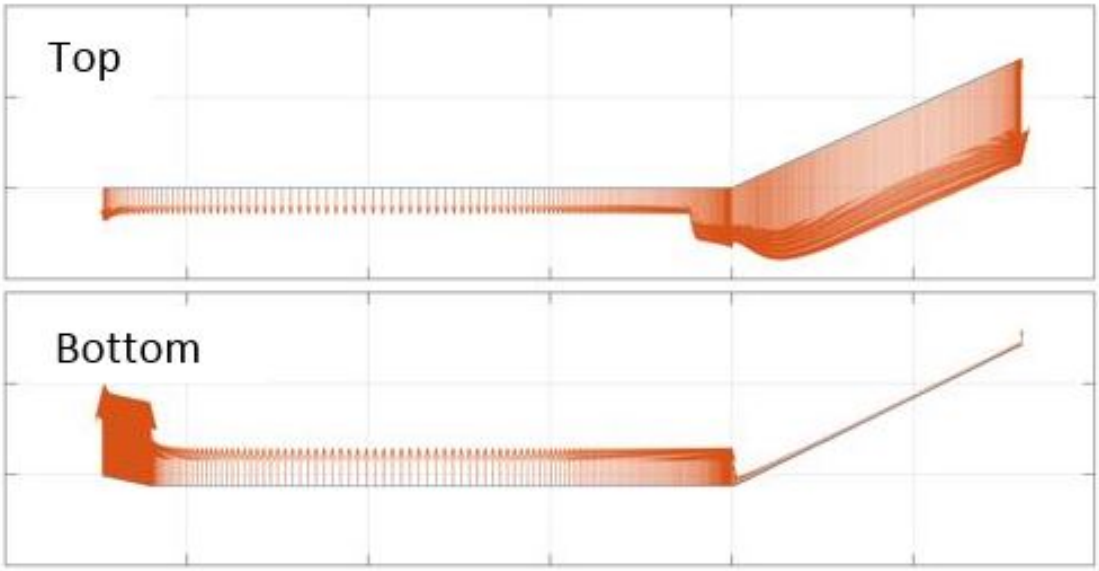

Figure 4.10: Pressure Distribution Normal to Surface for No Gap Case

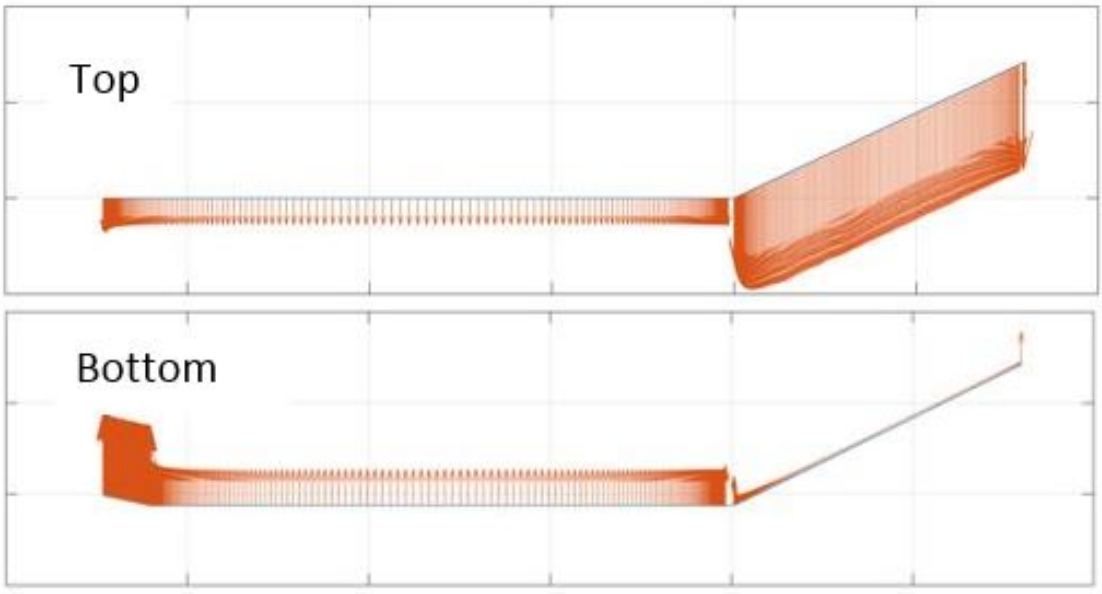

Figure 4.11: Pressure Distribution Normal to Surface for Gap Case

before being ejected up the ramp. The nature of these structures pulled flow toward defined lines, called lines of coalescence, creating streaks on the surface of the ramp. These streaks have a notable effect on the surface and can be seen in Figures 4.13a and 4.14a for skin friction coefficient and Mach number. The blue areas in this figure correlate to the lines of coalescence from Figure 4.12a. This phenomena is caused by separation created by the fluid being lifted off the ramp by counter-rotating vortices on either side of the line of coalescence. The formation of three-dimensional fluid structures and coalescence lines is not uncommon for SWBLI, and for a Mach number and ramp angle this high, it is to be expected. However, as Figure 4.12b shows, when a gap is added at the corner. These phenomena go away. The figure shows streamlines were similarly initiated, but as they approached the corner they continued with their trajectory, showing no deviation in the Z direction. Streamlines very close to the wall were pulled into the gap, recirculated, and ejected into the freestream below the ramp. Streamlines outside the boundary layer of the flat plate simply traveled over the gap and up the ramp. The results of this more linear and straightforward progression of air through the geometry can be seen in Figures 4.13b and 4.14b. It can be seen that no effects of Mach number and skin friction coefficient increase are registered ahead of the gap. Behind the gap there are no streaks discernable on the surface of the ramp.

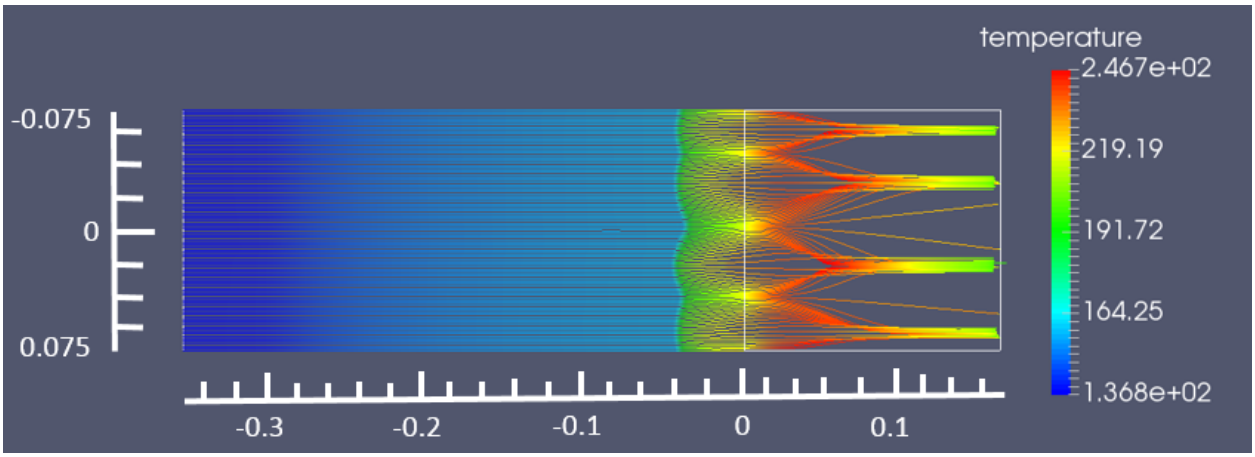

(a) No Gap

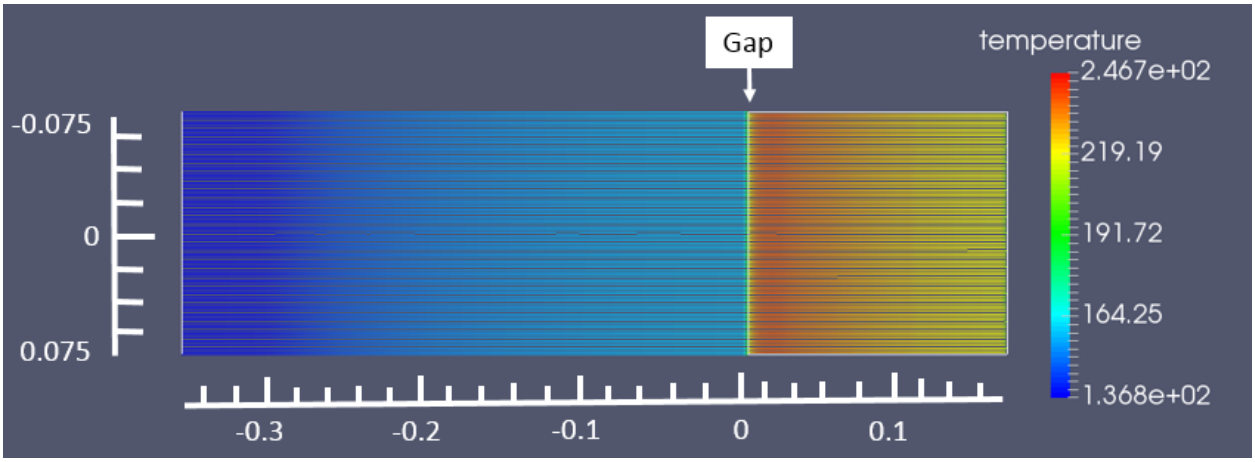

(b) Gap Case

Figure 4.12: Streamlines on Upper Surfaces

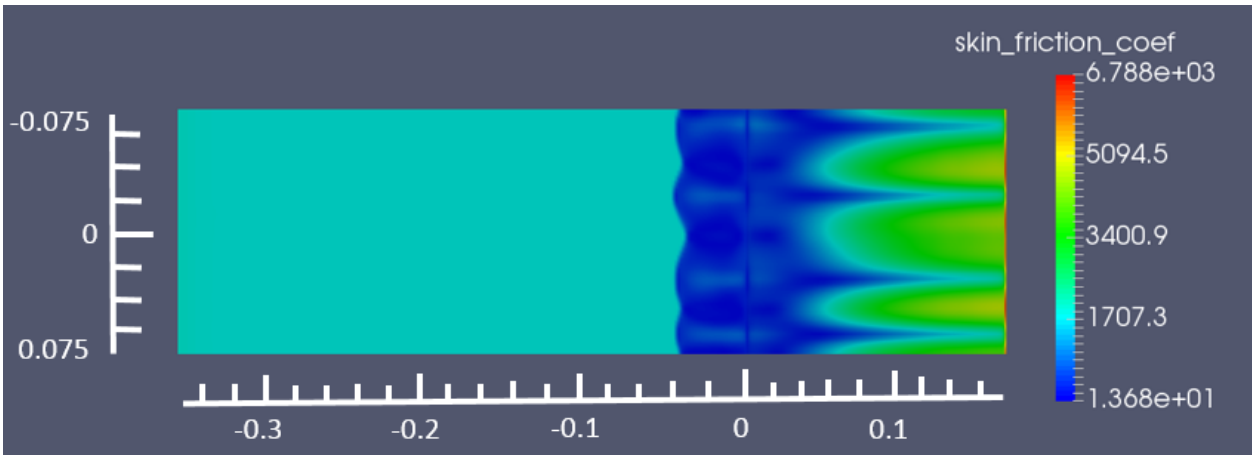

(a) No Gap Case

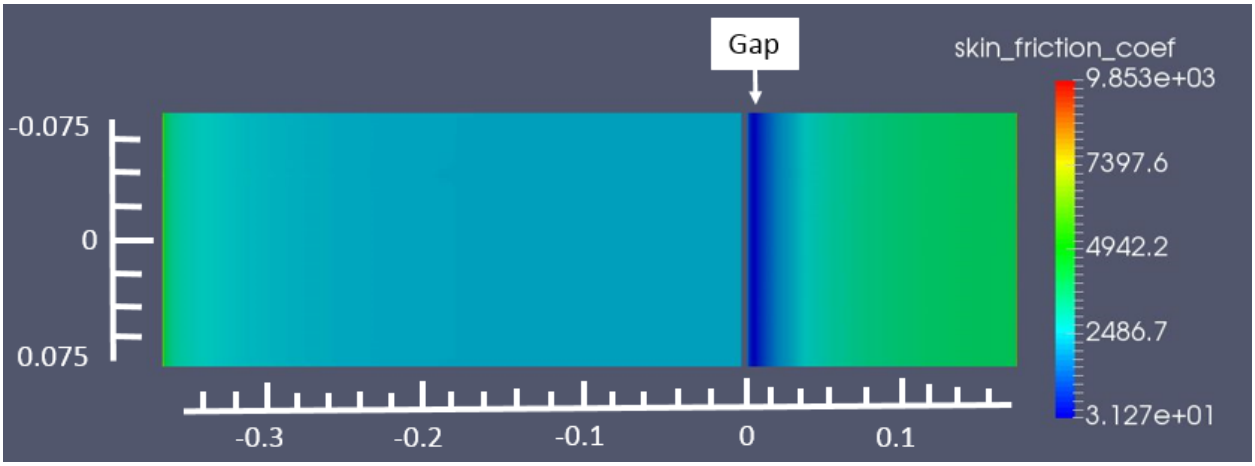

(b) Gap Case

Figure 4.13: Skin Friction Coefficient Contours on Surface of Flat Plate and Ramp

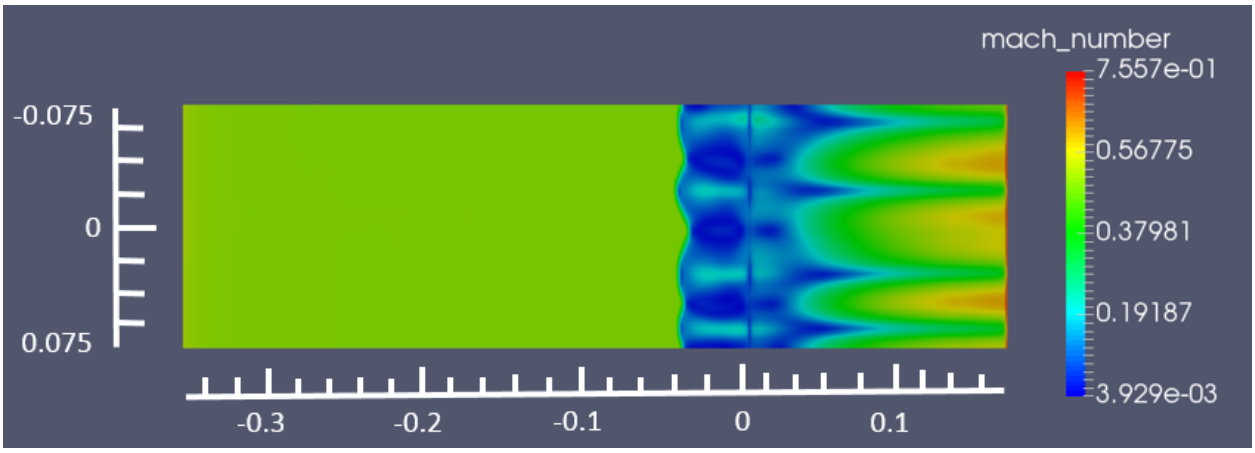

(a) No Gap Case

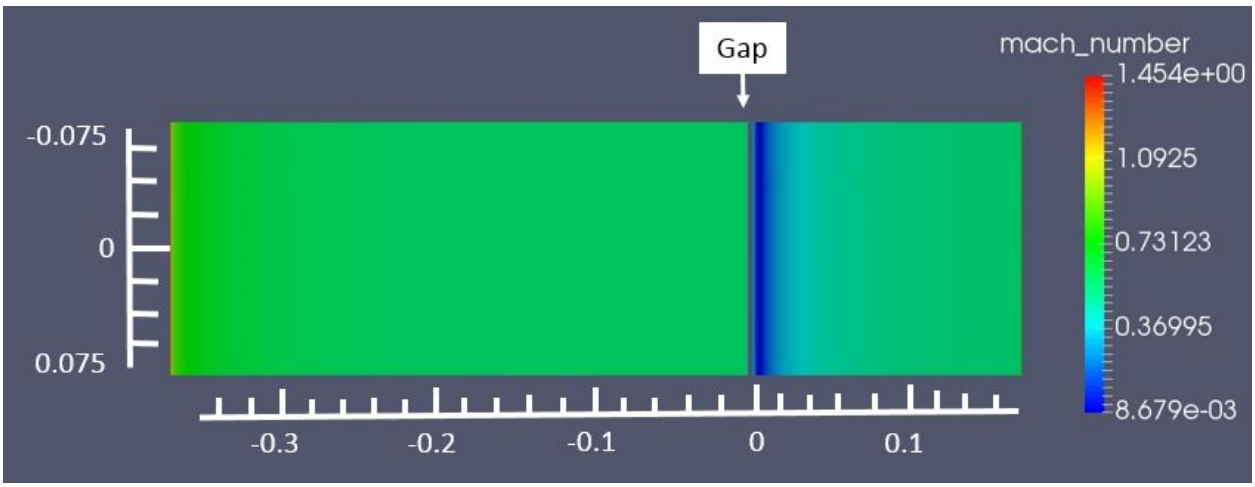

(b) Gap Case

Figure 4.14: Mach Number Contours on Surface of Flat Plate and Ramp

Chapter 5

Additional Test Cases

In any flight regime a wing, stabilizer, or control surface will encounter angles of attack other than 0°, and for this research it was important to understand how the angle of the incoming air would affect the SWBLI with and without compression ramp corner gap. Two angles, 2.5° and 5° were measured against a 0° setup. Reports for surface pressure, temperature, and skin friction were again created to compare the Gap and No Gap cases. The ramp angle of 24° and gap width non-dimensionalized by wing thickness of 0.4 remained constant. As a natural precursor to the angle of attack comparison test, a study of how incoming boundary layer height affects the SWBLI is presented. Finally, a test with a simulation of Mach 5 flow over a compression ramp is performed and documented.

5.1 Angle of Attack Comparison at Mach 3

5.1.1 Setup

Previous tests of the Full Domain geometry used inlets attached to the upper and lower flat plates. This simulated the effect of having a long wall ahead of the corner in which the large boundary layer could be generated. For the angle of attack comparison, however, the "wing" must stand alone in the airflow. Therefore, a new geometry had to be designed that included a leading edge for the wing. As a result, the flat plate would not be representative

of a section of tunnel floor, and the boundary layer on the flat plate would be much smaller. In turn the SWBLI recirculation region would be smaller too.

Since the new model did not have the same boundary layer height as [19], the minimum spacing near the wall to achieve a y^+ value of 1 had to be changed. A minimum wall spacing of $4.07 \cdot 10^{-8}$ m and a boundary layer thickness of 0.0036 m were calculated. The flow and boundary conditions remained consistent from the previous case with the exception of the inlet condition direction. To vary the angle of attack the incoming flow direction was changed.

Figures 5.2 and 5.3 show the result of removing the inlet profile boundary layer and allowing the height of the boundary layer to be determined by growth on the flat plate. In 5.2, the No Gap case comparison shows how much the boundary layer height affects the size of the SWBLI. The area taken up by the recirculation region is much larger for the larger boundary layer. However, in the Gap case there is very little visual change on the upper half of the domain and in the SWBLI region. This effect can most likely be attributed to where the shocks are formed in both cases. In the No Gap case, the shock is formed by smaller coalescing shock lines from the recirculation region. So, the larger the boundary layer, the longer the area that is available for coalescing shock lines to form. However, with the two Gap cases the shock impinges from the corner of the ramp without regard to the size of the boundary layer.

To more deeply understand how the boundary layer change affects the SWBLI and the affects generated on the plate and ramp, surface pressure distributions are plotted. For the No Gap case, Figure 5.4a shows that the separation point changes from X = -0.045m to X = -0.025m and that the pressure level increases to the max P_W/P_{inf} of 4.4 at a point on the ramp approximately 0.05m closer to the corner. For the Gap case, Figure 5.4b shows that the point on the flat plate where pressure increases is the same for both incoming boundary layers. Similarly, the smaller boundary layer case reaches the max P_W/P_{inf} sooner but, overall, the two plots are nearly identical. A close-up at the corner for the meshes of the full domain No Gap and Gap cases is shown in Figure 5.1.

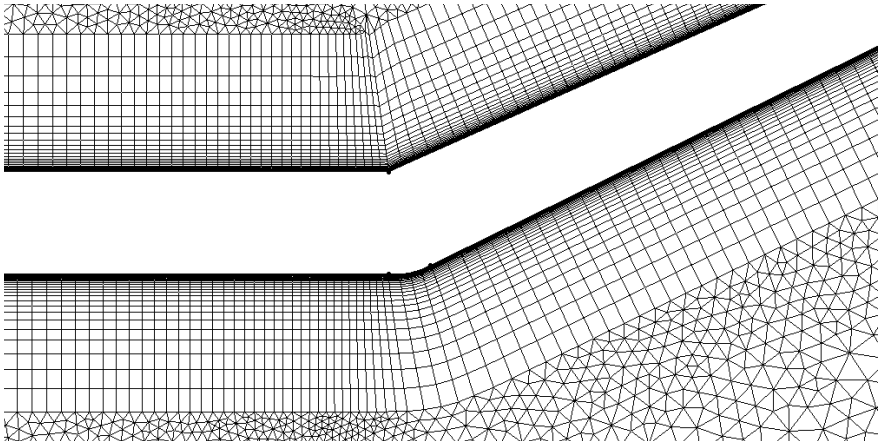

(a) No Gap Case Mesh

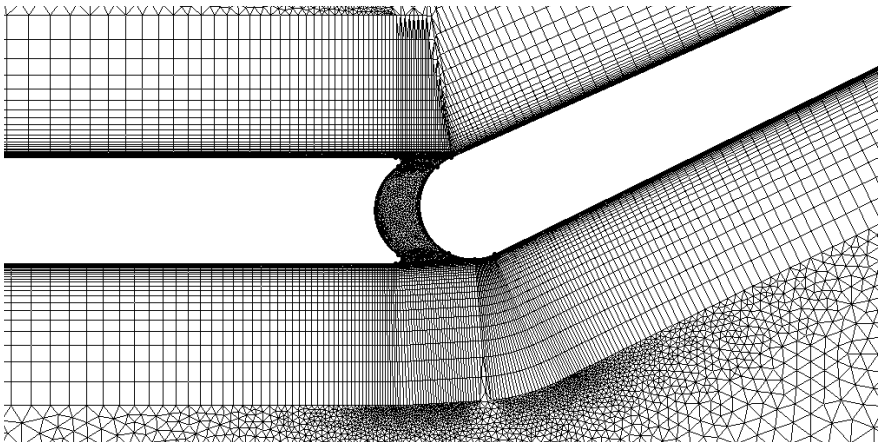

(b) Gap Case Mesh

Figure 5.1: Close-up of Full Domain Meshes.

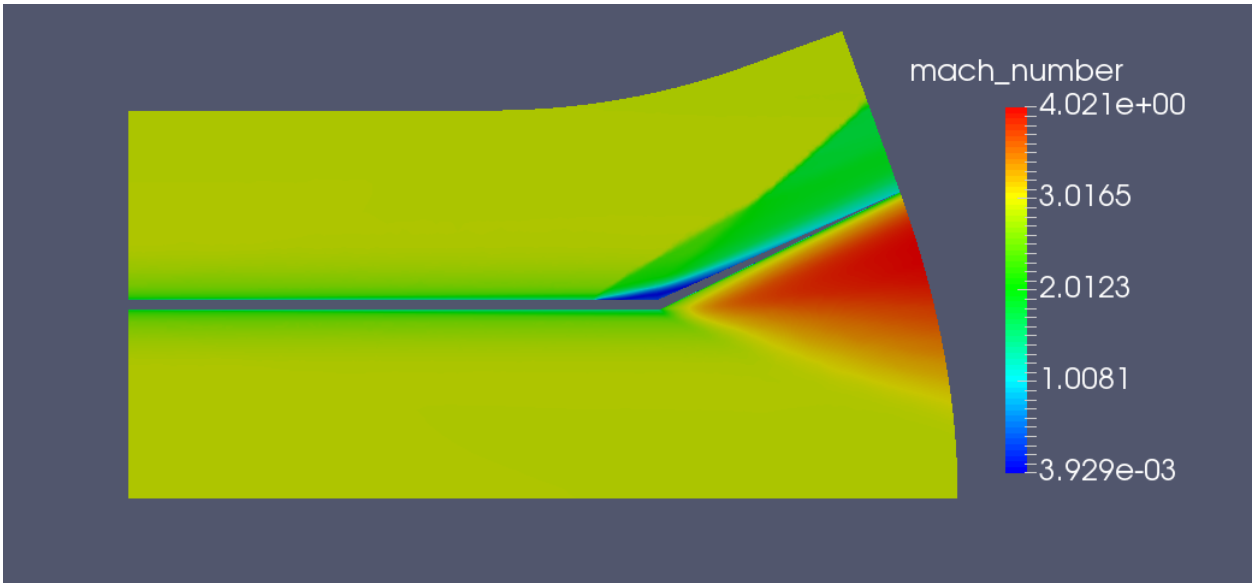

(a) No Gap Case with Incoming Boundary Layer

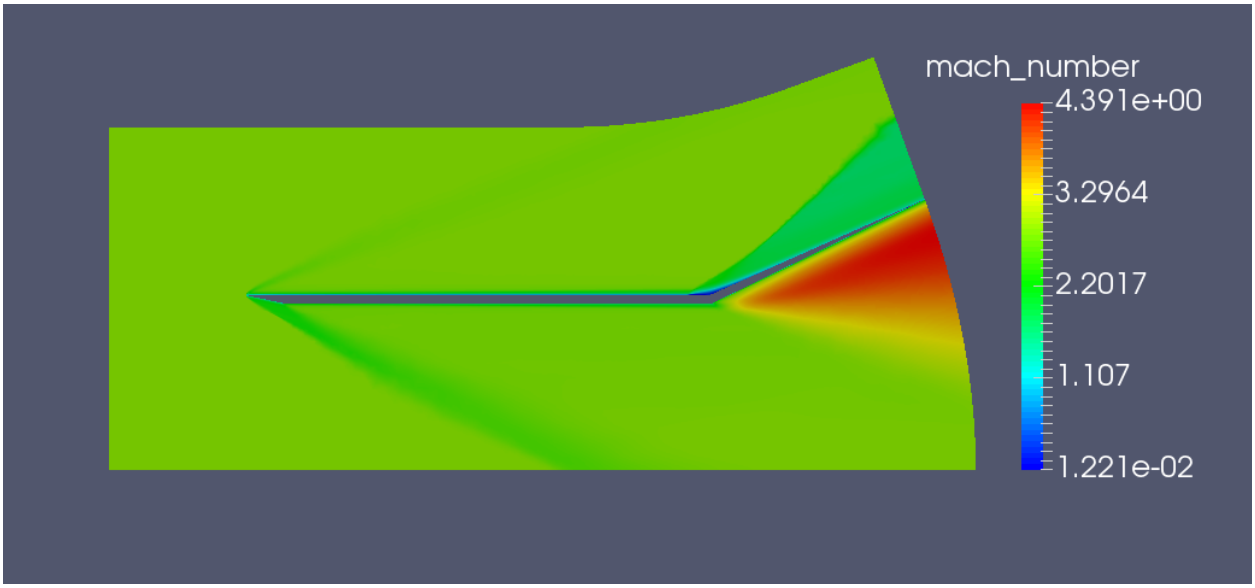

(b) No Gap Case without Incoming Boundary Layer

Figure 5.2: No Gap Case Full Domain Mach Number Contours for Boundary Layer Height Change

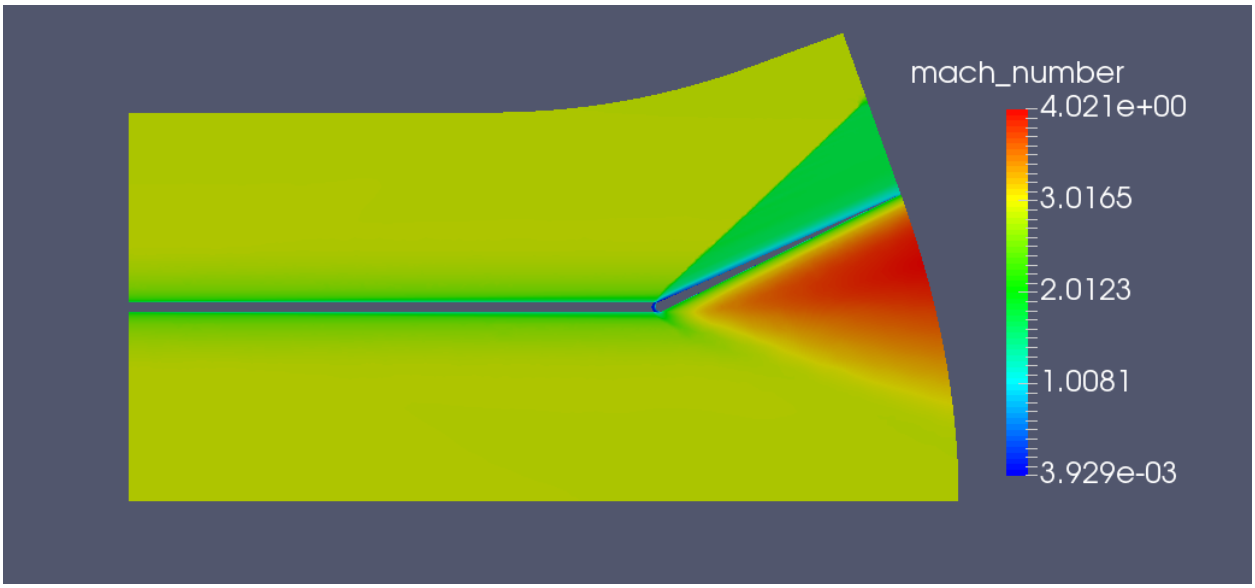

(a) Gap Case with Incoming Boundary Layer

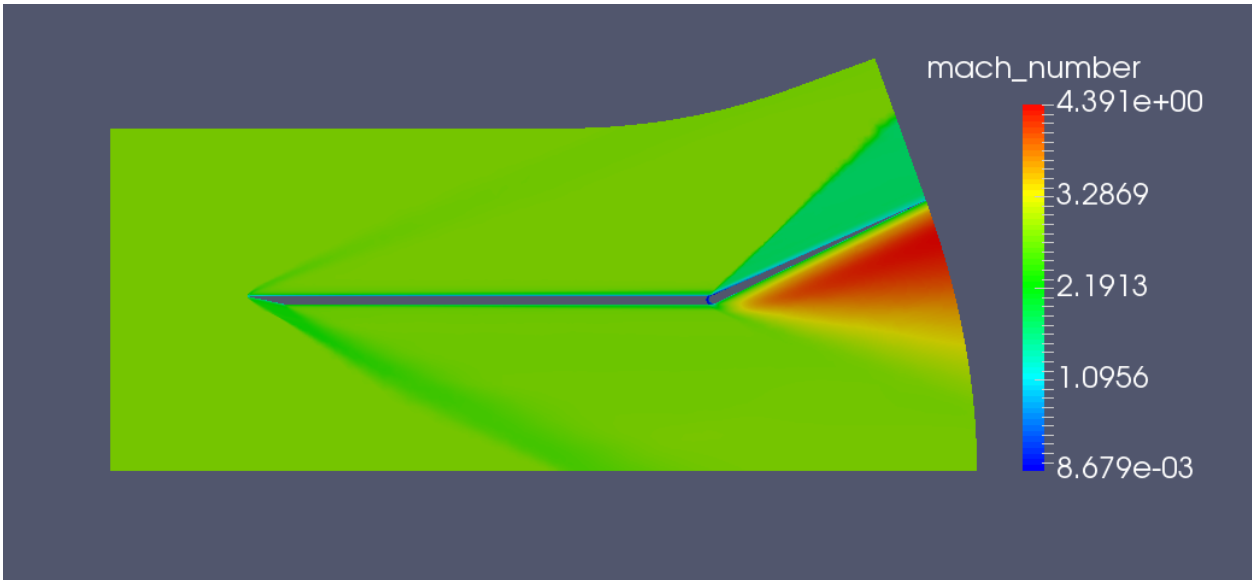

(b) Gap Case without Incoming Boundary Layer

Figure 5.3: Gap Case Full Domain Mach Number Contours for Boundary Layer Height Change

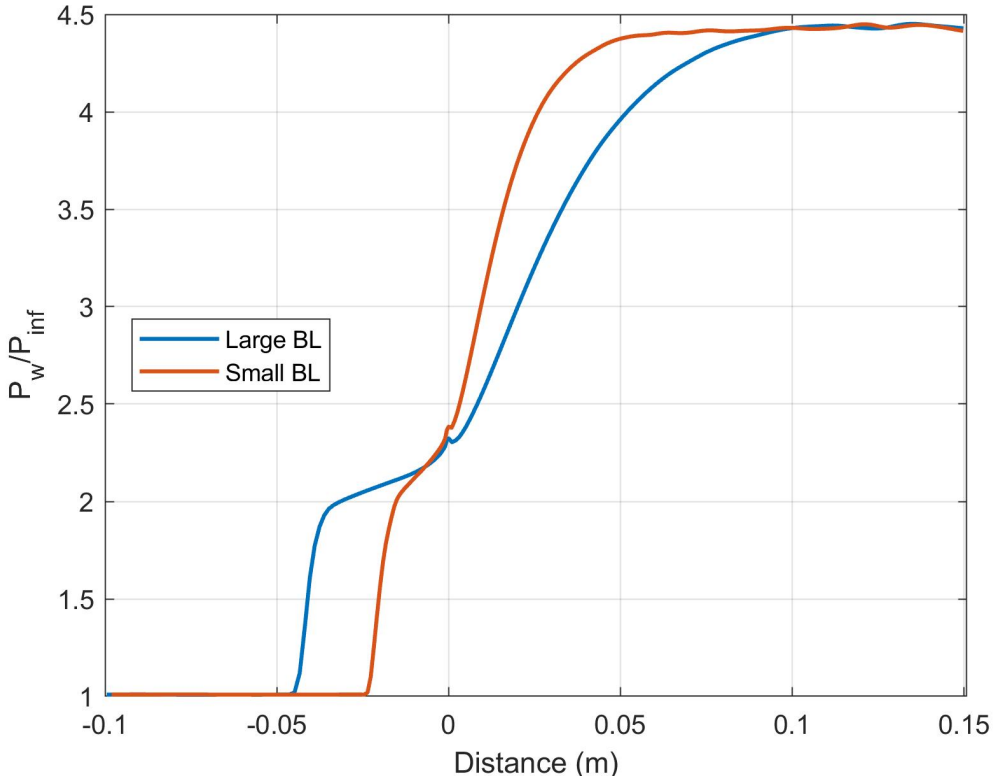

(a) Mach 5 No Gap Case Temperature

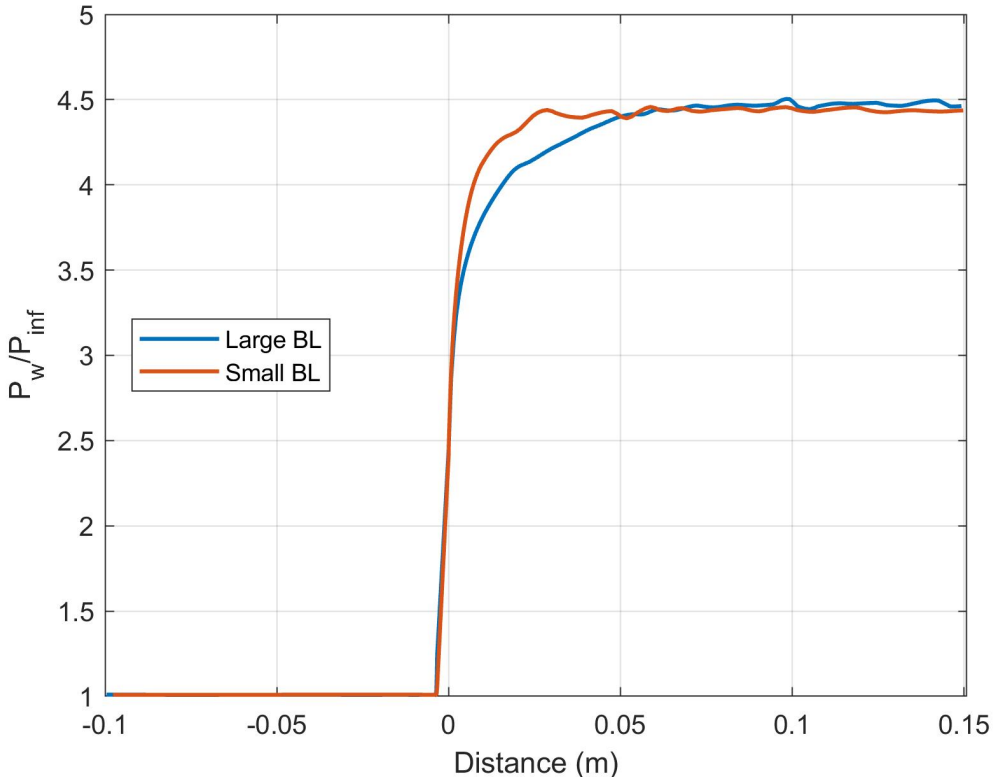

(b) Mach 5 Gap Case Temperature

Figure 5.4: Boundary Layer Height Comparison Effect on Surface Pressure Distribution

5.1.2 Results

After the new geometry with the leading edge on the wing was tested and the effect of changing the boundary layer height was understood, an angle of attack analysis was performed. The new geometry was tested at angles of 2.5° and 5° and compared against the 0° baseline case. To change the angle of attack, the X and Y components of velocity for the inlets were adjusted accordingly. Their results are shown for surface pressure distribution, surface temperature distribution, and skin friction coefficient, respectively. Figures 5.5, 5.6, and 5.7 show the comparison of the three angles of attack in the No Gap case. The trends in the plots remain consistent as the angle of attack changes. As angle increases, the pressure on the upper surfaces decreases. The temperature and skin friction coefficient decrease too. Separation point, as noted in Figure 5.5 stays the same for all three angles. When the gap is added the trends continue to hold. This is shown in 5.8, 5.9, and 5.10. There is a slight difference in the separation point and an uncharacteristic peak in the temperature plot for the highest angle, but the distance the separation point moved was only 0.0005 m. This effect could be more detrimental at higher angles of attack, but it cannot be inferred here. One important point to note in the angle of attack comparison is the behavior of flow in the high angle Gap case. The flow under the wing does not go into the gap, even as the flow direction points more directly at it. The recirculation region keeps air flow from entering the gap from the underside of the wing.

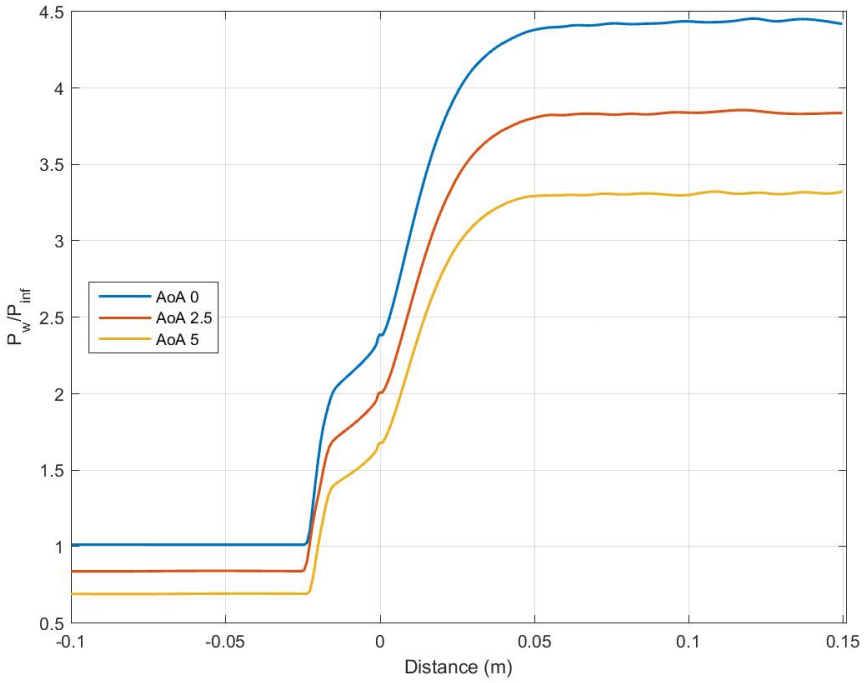

Figure 5.5: No Gap α Comparison on Surface Pressure Distribution

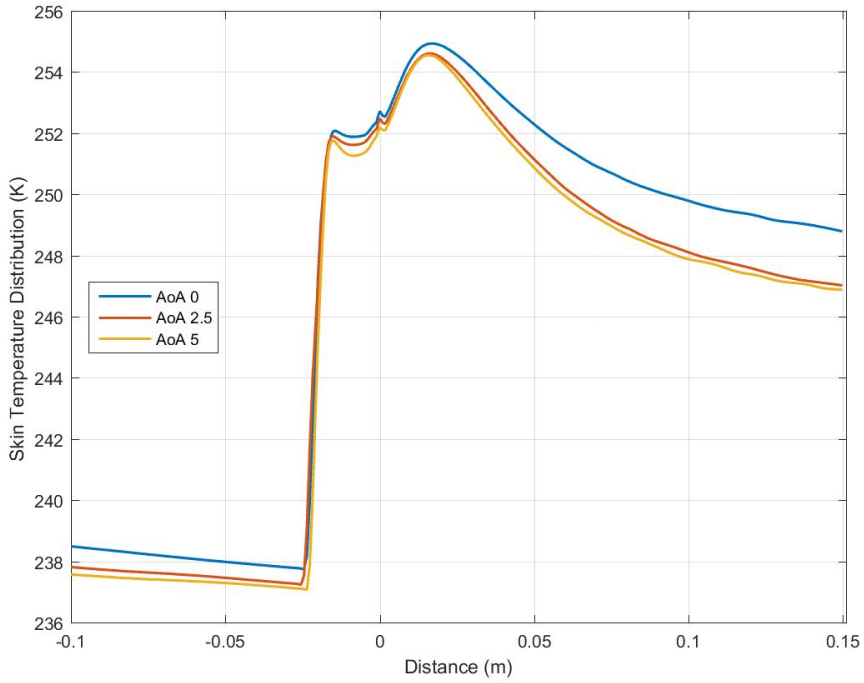

Figure 5.6: No Gap α Comparison on Surface Temperature Distribution

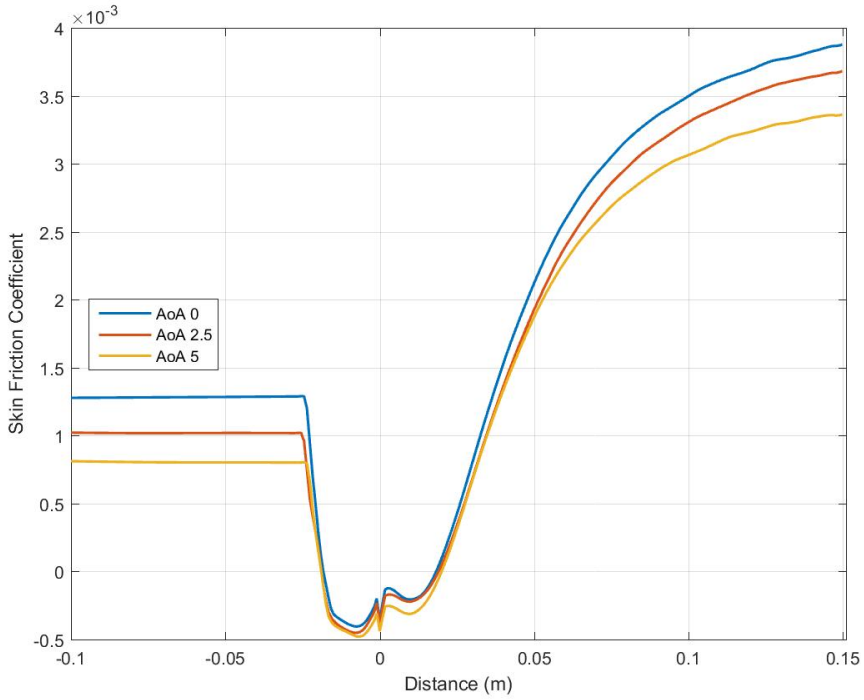

Figure 5.7: No Gap α Comparison on Surface Skin Friction Coefficient Distribution

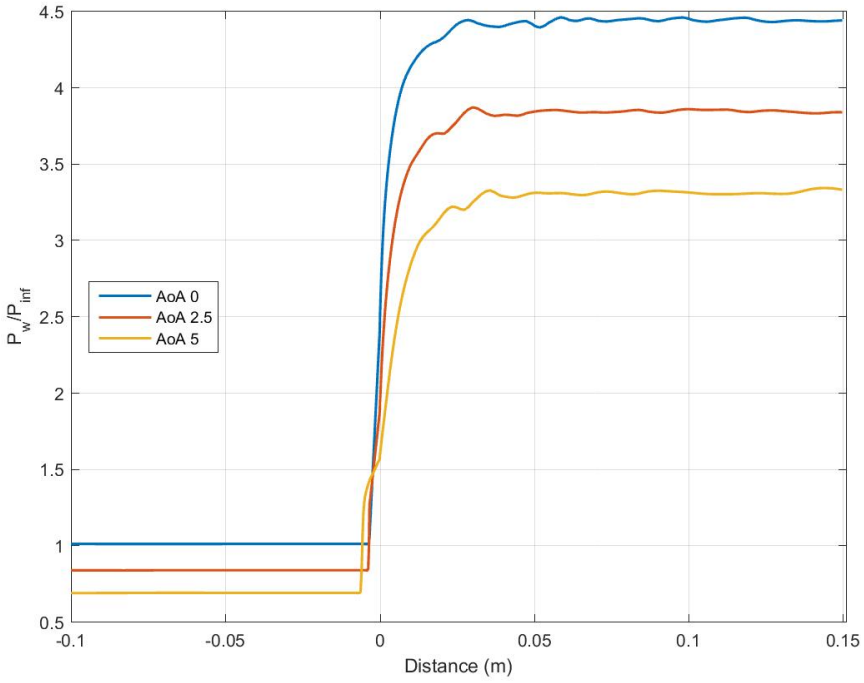

Figure 5.8: Gap α Comparison on Surface Pressure Distribution

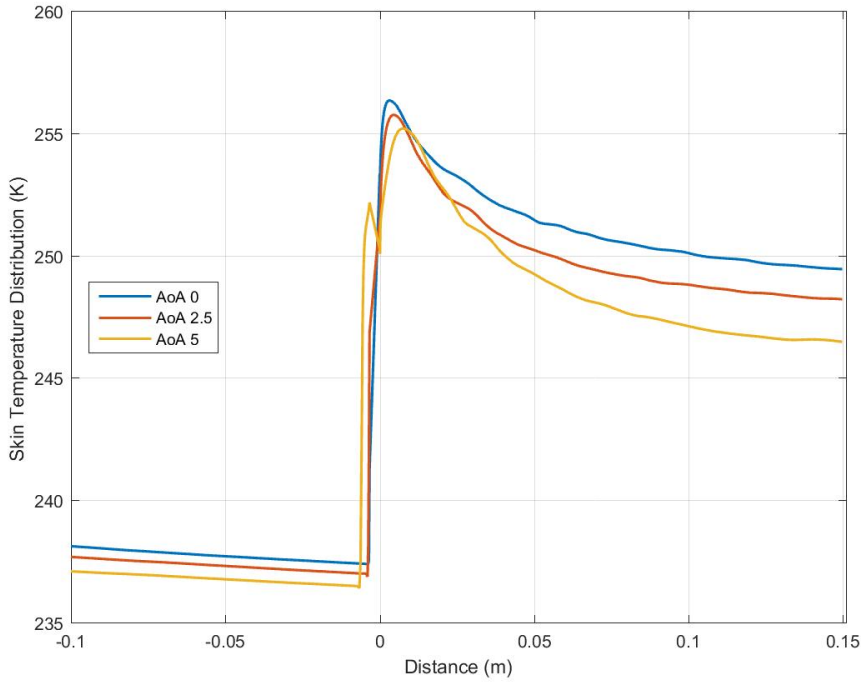

Figure 5.9: Gap α Comparison on Surface Temperature Distribution

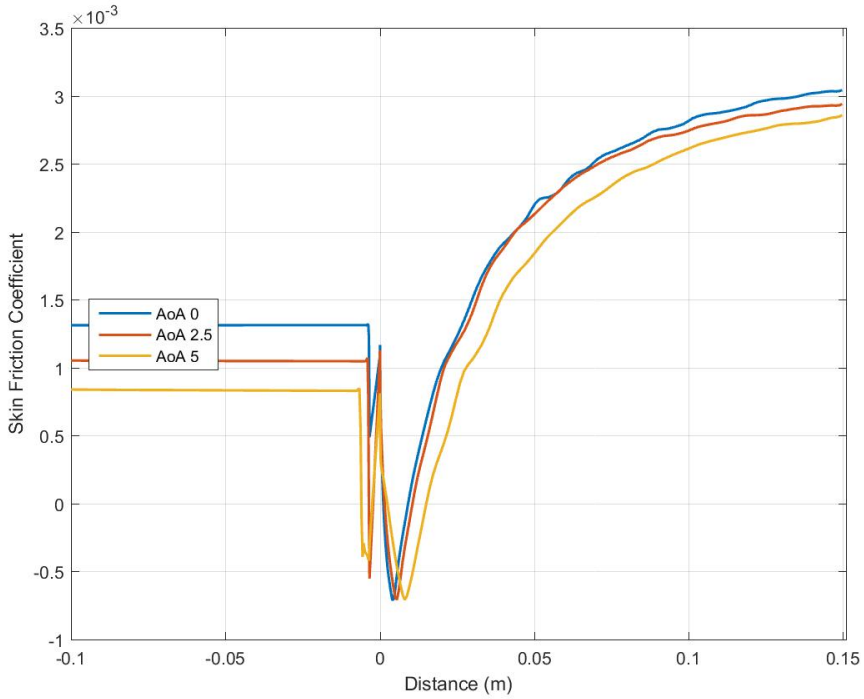

Figure 5.10: Gap α Comparison on Surface Skin Friction Coefficient Distribution

5.2 Flow Comparison at Mach 5

After examining the effect of angle of attack and boundary layer height on the gap, the effect of increasing the Mach number to 5 was studied. A Mach 5 test was chosen as a point of investigation because at this Mach number the supersonic regime begins to transition to the hypersonic [3].

5.2.1 Setup

The initial boundary conditions were pulled from the work of Edwards and Choi [15]. They are represented in Table 5.1. The static pressure and temperature were calculated by isentropic relations to be P = 4348.6 Pa and T = 59.3 K. The boundary layers were allowed to grow from the front of the flat plates instead of using preset boundary layer profiles.

5.2.2 Results

Figure 5.12 shows the results of adding the gap for Mach 5 flow through the domain. The higher Mach number led to a large recirculation region in the No Gap case and the Gap case again shows the disapearance of the corner recirculation region. Figures 5.13, 5.14, and 5.15 shows the span-wise averaged surface pressure, temperature, and skin friction coefficient. The results shown in these figures follow the same trends as the tests at Mach 3. Greater temperature and pressure jumps are seen at the shock for both cases, while the relative effect of gap remains the same. This shows that in the supersonic range under these flow conditions the effectiveness of the gap is unaltered.

The higher Mach number does allow an opportunity to return to the study of the Görtler vortices. The intensity of the magnitude of the vortex rotation increases with the higher velocity flow. As mentioned in the literature review in Chapter 2, the method developed by Navarro and Martinez [29], the ramp angle, separation point, and reattachment point are used to estimate the radius of curvature for the tube-like vortices created by the SWBLI. This method was applied to the Mach 5 No Gap case. The separation point and reattachment point were extracted from the surface pressure distribution plot in Figure 5.13 and were

Table 5.1: Free-Stream and Boundary-Layer Properties Mach 5

Case	M_∞	$U_\infty, m/s$	P_0, Pa	T_0, K	P, Pa	T, K
Based on [15].	4.95	764	$2.17 \cdot 10^6$	350	4348.6	59.3

-0.032 m and 0.058 m, respectively. The radius for this case was then calculated as 0.33 m. The vortices themselves are shown in Figure 5.11.

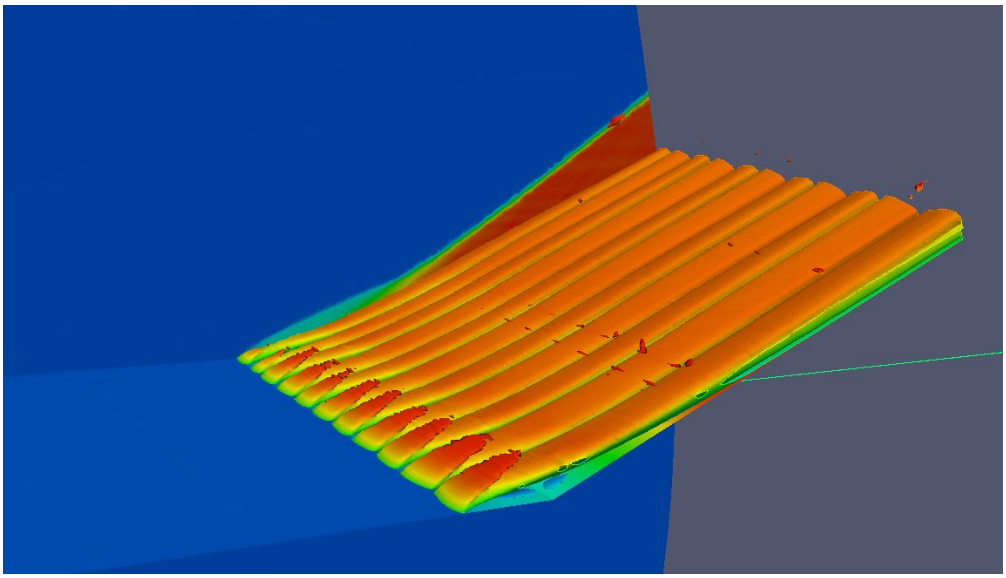

Figure 5.11: Counter-rotating vortices on Mach 5 Ramp.

The irregularities of the flow, the rotational nature of the Görtler vortices, and the streaks of increased friction on the surface due to up wash of flow between vortex tubes all disappear with the addition of the gap. The complex nature of air created by the SWBLI behind the ramp becomes simplified and more predictable. The uneven and oscillating shape of separation line created on the flat plate in the span wise direction in the No Gap case becomes a straight, predictable line. The inherent three dimensionality of the vortices and interaction region gave way to flow behavior that stays constant down the length of the span.

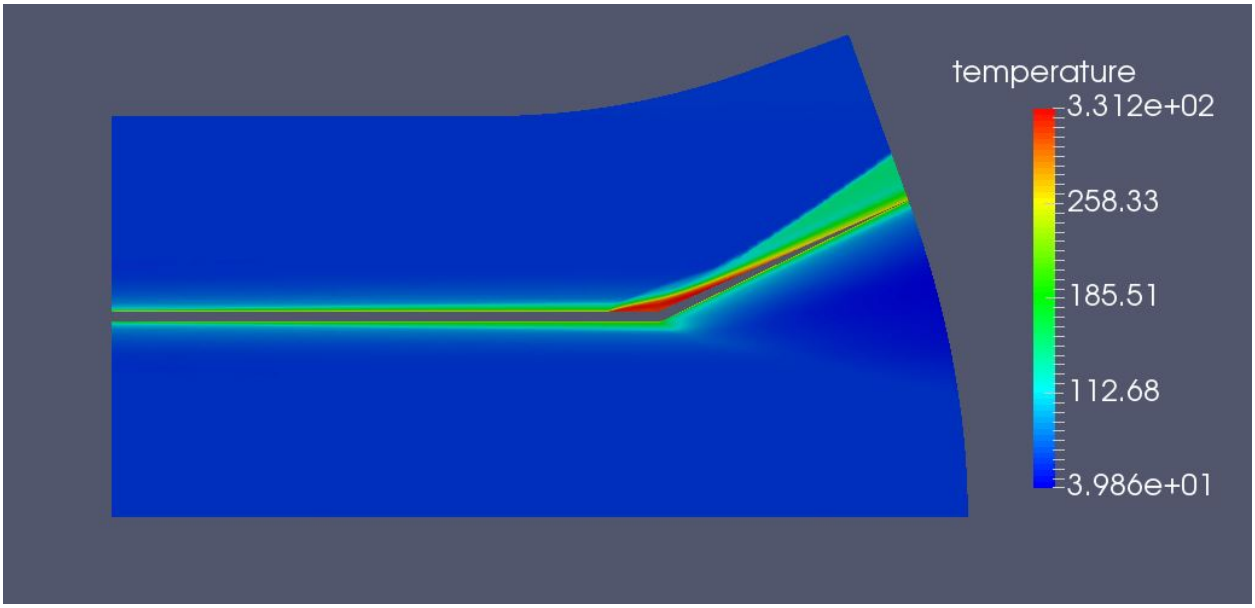

(a) No Gap Case

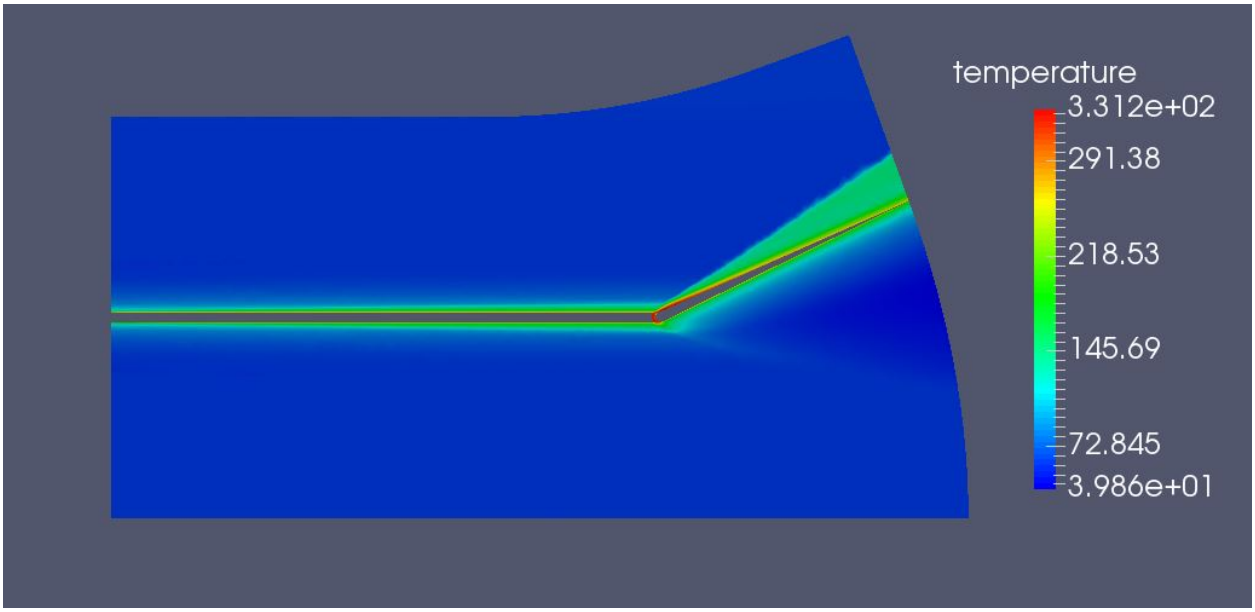

(b) Gap Case

Figure 5.12: Full Domain Temperature (K) Contours For Mach 5.

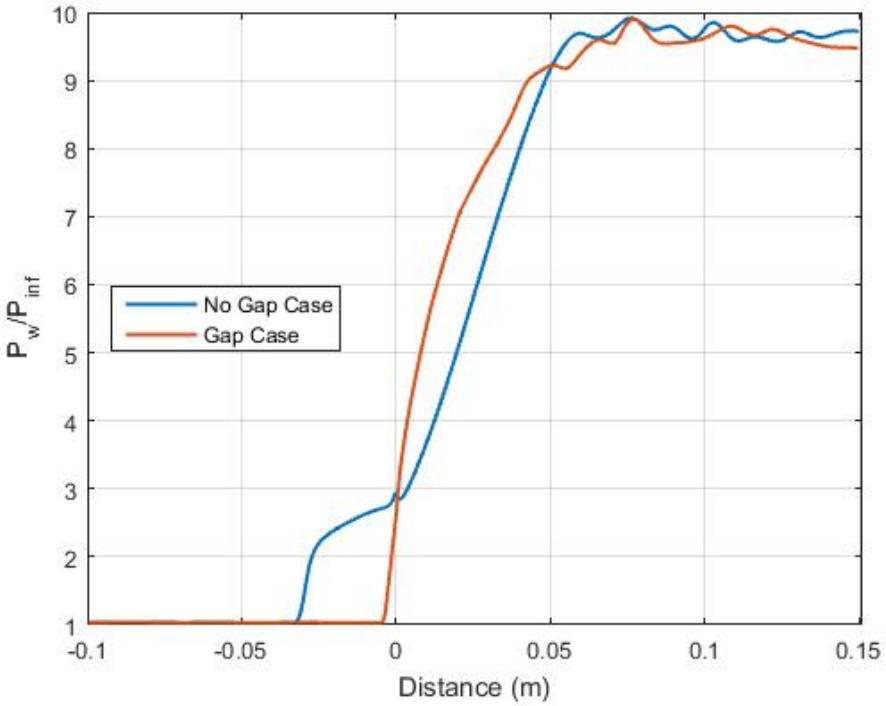

Figure 5.13: Mach 5 Surface Pressure Distribution

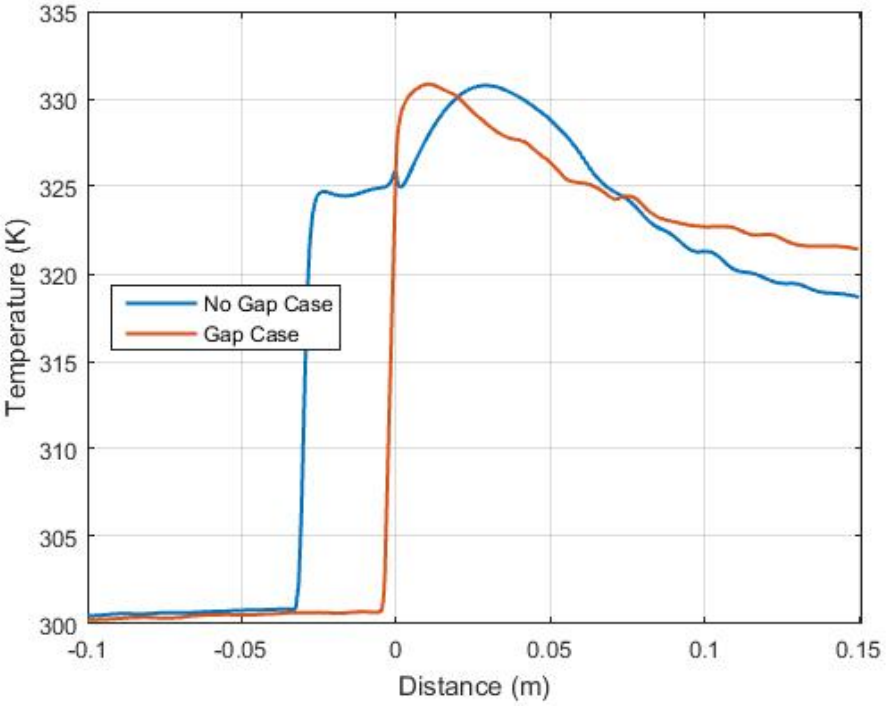

Figure 5.14: Mach 5 Surface Temperature Distribution

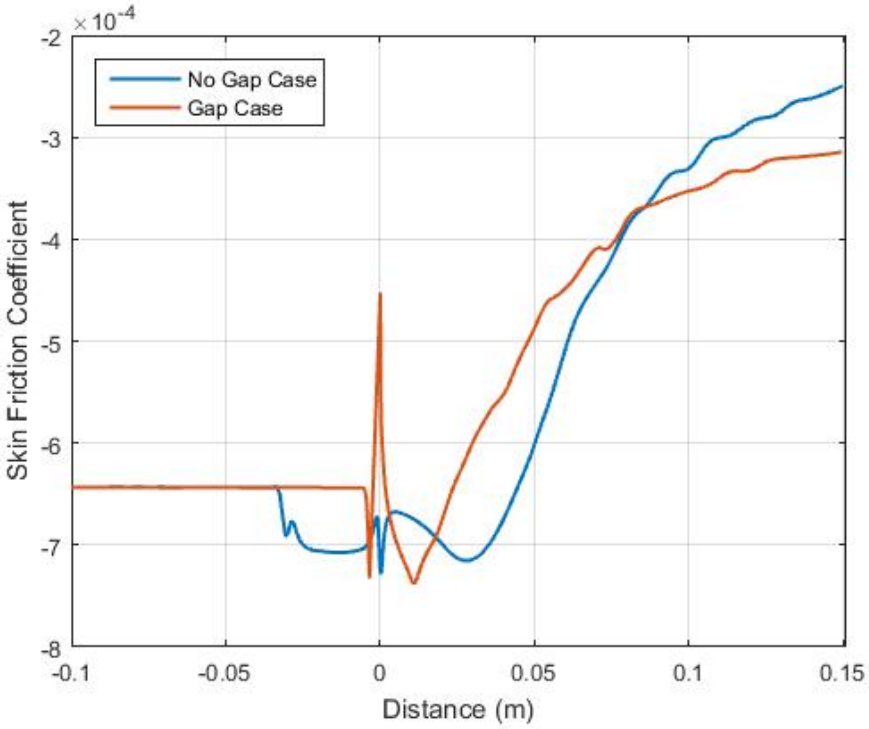

Figure 5.15: Mach 5 Surface Skin Friction Coefficient Distribution

Chapter 6

Conclusions

This research began with a problem statement: SWBLI can create damaging effects on the surfaces of a compression ramp. Would introducing a hole in a wing or a gap at this corner help to mitigate this problem? The question introduced a slew of additional points of investigation. What would the gap look like? Would the gap mitigate the recirculation region but cause additional unforeseen problems? As other factors of geometry and flow change, what would be the response with the gap? The answers to these problems began to form with the study of existing literature. There are a number of methods currently used to change how SWBLI occurs on a ramp, including one study found that introduced a gap. Other literature helped to provide a groundwork for the current study by showing the conditions and procedures needed to create a simulation for SWBLI, the most crucial of these being the work of Gieseking et al. [19]. This study supplied the boundary conditions, geometry, and mesh characteristics to build a 3D, supersonic simulation, and it provided experimental and computational data for solution comparison.

A Half Domain case was built without a gap, a method was introduced that grew a boundary layer with recycling to match [19], and a RANS turbulence model was chosen. It was found that the RANS model provided an accurate enough simulation to match the data from [19]. From there, the Full Domain case was created, and after a design process occurred, a gap was added. Surface pressure distribution, surface temperature distribution, and surface skin friction coefficient were studied to compare the addition of the gap to the baseline case. It was found that the total amount of pressure added to the two upper surfaces

was very similar with only about 1% difference between the two cases. However, a study of the hinge moment about the corner of the wing found that the hinge moment was increased by nearly 12% for the Gap case. It is impossible to know without application whether this increased moment would be detrimental to a vehicle or not, but it would definitely have an impact on design. Temperature distribution was found to be much lower on the ramp, and the average of the applied temperature on the upper surfaces was found to be lower with the addition of the gap.

The largest discrepancy between surface effects for the No Gap and Gap cases in the surface skin friction coefficient. The No Gap case showed large streaks of alternating high and low friction on the ramp past the corner. A literature review and investigation of flow behavior during post-processing showed that this streaking is caused by a row of counter-rotating vortices created at the separation line because of the angle of curvature of the flow. The vortices lift and deposit air in an alternating pattern span wise on the ramp. The addition of the gap removed all of this behavior. It would be fair to say that any design based on the flow behavior on the ramp behind a compression corner would be made simplified by not having to account for these vortices. It was also discovered in the Mach 5 test that the number of these vortex pairs goes up with Mach number.

Additional cases for angle of attack and boundary layer height comparison showed that the trend shown in the baseline case stands for a variety of changes in the flow. As the angle of attack changed the pressure dropped an equivalent amount per angle, but the gap performed as expected. The pressure, temperature and skin friction effects left the flat plate alone while affecting the ramp in their own unique ways. The smaller boundary layer height produced a smaller SWBLI region, but the gap effects were the same. Finally, even as the Mach number approached the hypersonic regime the gap worked. The overall amount of pressure loading was left nearly untouched but the distribution changed. The average temperature on the surface was lower, and, as mentioned earlier, the streaks in skin friction were eliminated.

The goal of this study was to determine whether the gap would be a viable way to help mitigate the negative effects on a compression ramp caused by SWBLI. To this effect, the study was a success. While it was found that the pressure loading amount does not change

significantly, a result which was counter to initial guesses, the temperature and friction changes were positive. Also, there were no unforeseen consequences found in the flow or on the surface caused by the gap. The temperature in and around the gap was not beyond reason. The amount of increased moment on the wing was higher, but was only around 10% greater than that of the baseline. It can be concluded that adding a gap to a compression ramp corner can help mitigate and sometimes eliminate the detrimental effects of SWBLI.

6.1 Recommendations for Future Work

The present work has provided a description of how the addition of a gap at the foot of a compression ramp changes the effects of SWBLI by examining a number of variables. However, this work remained entirely steady state. There are a number of ventures for study that can be followed from the information found above. Recommendations for further study are summarized.

• First, the incoming Mach number and ramp angle could be changed to see how the gap would respond. It is was stated in [7] and [11] that these two features create the most predictable changes in the size of the SWBLI. The present work shows how flow at Mach 5 responds to the addition of gap, but further study would be beneficial to see how the addition performs at Mach numbers even higher than 5, going into the hypersonic regime. At that point, air chemistry effects come into play, and it would be interesting to see the response of the flow to the gap. Also, as ramp angle increases the recirculation region increases. Research could be performed starting at small angles and going up, when the angle is large enough for the gap to have a significant effect on the SWBLI.

• Next, the shape and size of the gap and the thickness of the wing structure could be changed to more robustly characterize the effect of the gap addition to SWBLI. At too large of a size the gap would create more secondary issues than would be solved by the mitigation of the SWBLI, and at too small of a size the gap would not allow full recirculation which currently allows flow to safely pass over the gap. The ball and socket connection was used here, but the connection design of plate and ramp could be changed. Additionally, the

geometry could be changed to represent an external feature of a fuselage or other aerodynamic body instead of a wing and control surface design.

• Finally, the most important addition to this research would be to study how the gap performs during a transient simulation. Many of the effects of SWBLI can be seen in their steady state response but realization of fully turbulent flow along the flat plate would change the response of the SWBLI. The RANS solver used in the current work does a good job of representing the average of the perturbations that fully turbulent flow causes but there are aspects of the SWBLI that are not found without this turbulence. Transient features like the large scale, low frequency "breathing" motion of the recirculation region along with the higher frequency vortex generation at the corner are under a great deal of scrutiny by the community [15]. It is known that the motion of the shock recirculation region create beat on the structure over time and can cause damage. It would be very interesting, then, to see how a corner gap of the style presented here would affect this motion. There are always ways to improve aerodynamic design as the aerospace engineering continues to push the bounds of flight, SWBLI will be a topic of investigation. This research gave a brief glimpse at some of the possible avenues for study in the future.

Bibliography

[1] Acquaye, F. K. (2016). The zero-divisor graph of a commutative ring, ii. *Lecture Notes in Pure and Applied Mathematics*, 220:61–72. 20

[2] Anderson, J. (2002). *Modern Compressible Flow: With Historical Perspective*. McGraw-Hill Education. 15

[3] Anderson, J. (2006). *Hypersonic and High-Temperature Gas Dynamics*. 52

[4] ANSYS, Inc. (2016). Ansys fluent users guide.pdf. Accessed: 09-Jun-2016. 20

[5] ANSYS, Inc. (2017). *Academic Research Fluent, Release 17.1*. Help System. ANSYS, Inc. 14

[6] Ariff, M. and Salim, S. (2009). Wall y+ approach for dealing with turbulent flow over a surface mounted cube: Part 1 - low reynolds number. *Seventh Internation Conference on CFD in the Minerals and Process Industries*. 8

[7] Campo, L. M., Eaton, J., Cappelli, M. A., and Iaccarino, G. (2014). *Effects of shock strength, confinement, and geometric perturbations on shock boundary layer interactions*. PhD thesis, Stanford University. x, 5, 6, 7, 59

[8] Candler, G., Nompelis, I., Druguet, M., Holden, M., Wadhams, T., Boyd, I., and Wang, W. (2001). Cfd validation for hypersonic flight - hypersonic double-cone flow simulations. *40th AIAA Aerospace Sciences Meeting & Exhibit, Aerospace Sciences Meetings*. 2

[9] Casper, K., Beresh, S., Henfling, J., Spillers, R., Pruett, B., and Schneider, S. (2016). Hypersonic wind-tunnel measurements of boundary-layer transition on a slender cone. *AIAA Journal*, 54 No. 4. 2

[10] Choi, J. (2009). Compressible boundary layer predictions at high reynolds number using les/rans models. *AIAA Journal*, 47:2179–2193. 9, 10, 22, 23

[11] Delery, J. and Dussauge, J. P. (2009). *Shock Waves*. Springer-Verlag. 3, 5, 6, 59

[12] Dolling, D. (2001). Fifty years of shock-wave/boundary-layer interaction research - what next? *AIAA Journal*, 39:1517–1531. 6

[13] Donaldson, C. (1950). Investigation of a simple device for preventing separation due to shock and boundary layer interaction. *NACA*. 3, 12

[14] Doppler, C. (1842). *Über das farbige Licht der Doppelsterne und einiger anderer Gestirne des Himmels*. 2

[15] Edwards, J., Choi, J., and J., B. (2008). Large-eddy/reynolds-averaged navier-stokes simulation of a mach 5 compression-corner interaction. *AIAA Jornal*, 46. 8, 10, 52, 53, 60

[16] Floryan, J. and Saric, W. (1982). Stability of Görtler vortices in boundary layers. *AIAA*, 20. x, 11, 36

[17] Fröhlich, J. and von Terzi, D. (2008). Hybrid les/rans methods for the simulation of turbulent flows. *Progress in Aerospace Sciences*, 44, Issue 5. 7

[18] Gerasimov, A. (2016). Quick guide to setting up les-type simulations. 15

[19] Gieseking, D., Edwards, J., and Choi, J. (2011). Simulation of a mach 3 24-degree compression-ramp interaction using les/rans models. *47th AIAA/ASME/SAE/ASEE Joint Propulsion Conference and Exhibit*. x, 3, 4, 5, 7, 10, 14, 15, 17, 19, 20, 22, 23, 43, 57

[20] Inger, G. and Zee, S. (1978). Transonic shock/turbulent boundary layer interaction with suction or blowing. *Journal of Aircraft*, 15. 3, 12

[21] Kendall Jr., J. (1956). *An Experimental Investigation of Leading Edge Shock Wave-Boundary Layer Interaction at Hypersonic Speeds*. PhD thesis, California Institute of Technology. 3

[22] Mack, A., Schfer, R., Glhan, A., and Esser, B. (2004). Flowfield topology changes due to fluid-structure interaction in hypersonic flow using ansys and tau. *Notes on Numerical Fluid Mechanics and Multidisciplinary Design New Results in Numerical and Experimental Fluid Mechanics*, IV:196–203. x, 3, 12, 13, 26

[23] Martos, J. (2017). *Aerothermodynamic Design, Manufacturing and Testing of a 3-D Prototype Scramjet*. PhD thesis, Instituto Tecnológico de Aeronáutica. x, 8

[24] Mathews, D. (1969). *Shock-wave/boundary layer interactions in two-dimensional and axially-symmetric flows including the influence of suction.* PhD thesis, University of Washington. 3, 12

[25] McCormick, D. (1993). Shock/boundary-layer interaction control with vortex generators and passive cavity. *AIAA Journal*, 31 No. 1. 3, 12

[26] Minwei, W. and Martin, M. (2007). Direct numerical simulation of supersonic turbulent boundary layer over a compression ramp. *AIAA Journal*, 45 No. 4. 2

[27] MIT Department of Ocean Engineering (2004). Marine hydrodynamics lecture 17. 15

[28] NASA Langley Research Center (2015). The menter baseline turbulence model. 19

[29] Navarro-Martinez, S. and Tutty, O. (2005). Numerical simulation of gortler vortices in hypersonic compression ramps. *Computers and Fluids*, 34. x, 11, 12, 52

[30] Saad, M. (2013). *Experimental Studies on Shock Boundary Layer Interactions using Micro-ramps at Mach 5.* PhD thesis, University of Manchester. 6, 12

[31] Schultz, M., Finlay, J., Callow, M., and Callow, J. (2003). Three models to relate detachment of low form fouling at laboratory and ship scale. *Biofouling*, 19. x, 8, 9

[32] Settles, G. (1994). Supersonic and hypersonic shock / boundary layer interaction database. *AIAA Journal*, 32 No. 7:1377–1383. 9, 10, 22, 23

[33] Shin, J., Narayanaswamy, V., Laxminarayan, R., and Clemens, N. (2007). Characteristics of a plasma actuator in mach 3 flow. *45th AIAA Aerospace Sciences Meeting & Exhibit, Aerospace Sciences Meetings.* 2

[34] Spalart, P. and Allmaras, S. (1992). A one-equation turbulence model for aerodynamic flows. *AIAA.* 20

[35] Squire, L. (1970). Further experimental investigations of compressible turbulent boundary layers with air injection. *Aeronautical Research Council R&M*, 3627. 3, 12

[36] Thomas, G. (1976). Compressible turbulent boundary layers with combined air injection and pressure gradient. *Aeronautical Research Council R&M*, 3779. 3, 12

Vita

Andrew Brandon Bell, son of Nancy Bell, was born in Flowood, Mississippi on August 15, 1994. He graduated from St. Aloysius High School in May 2012. The following August he enrolled at Mississippi State University. In May 2016, he graduated with a Bachelor of Science degree from the Department of Aerospace Engineering. In August of 2016, he began an aerospace engineering graduate degree program at the University of Tennessee Space Institute and received a Masters of Science in May of 2018. Andy is now working as an applied aerodynamics engineer for Dynetics in Huntsville, Alabama. He lives happily with his wife, Mallory; son, Noah; and dog, Kota.